Assessing runoff generation in riparian wetlands: monitoring groundwater-surface water dynamics at the micro-catchment scale

B. Scheliga[1], D. Tetzlaff [3,2,1], G. Nuetzmann[2] and C. Soulsby [1,2]

[1] Northern Rivers Institute, School of Geosciences, University of Aberdeen, AB24 3UF, UK.

[2] Leibniz Institute of Freshwater Ecology and Inland Fisheries, Berlin, 12587, Germany.

[3] Department of Geography, Humboldt University Berlin, Berlin, 10099, Germany.

Corresponding author: B. Scheliga, Bernhard.scheliga@abdn.ac.uk, +441224 272338

ORCiD:

B. Scheliga: 0000-0003-2764-6605

D. Tetzlaff: 0000-0002-7183-8674

C. Soulsby: 0000-0001-6910-2118

Abstract

Riparian wetlands (RW) are important variable source areas for runoff generation. They are usually characterised by a combination of groundwater exfiltration - which maintains saturated conditions in low-lying organic-rich soils - and direct precipitation. Both processes interact to generate overland flow as a dominant runoff process. The small-scale details of groundwater-surface water (GW-SW) interactions are usually not well understood in RW. Here, we report the results of a study from an experimental catchment in the Scottish Highlands where spatio-temporal runoff processes in RW were investigated using isotopes, alkalinity and hydrometric measurements. We focused on perennial micro-catchments within the RW and ephemeral zero-order channels draining peatland hollows and hummocks to better understand the heterogeneity in GW-SW interactions. The 12-month study period was dominated by the wettest winter (Dec/Jan) period on record. Runoff generation in the RW was strongly controlled by the local groundwater response to direct rainfall, but also the exfiltration of groundwater from upslope. This groundwater drainage is focused in the hollows in ephemeral and perennial drainage channels, but in wet conditions, as exfiltration rates increase, can affect hummocks as well. The hollows provide the dominant areas for mixing groundwater, soil water and direct rainfall to deliver water to the stream network as hollows "fill and spill" to increase connectivity. They also provide wet areas for evaporation which is evident in enriched isotope signatures in summer. Although there is some degree of heterogeneity in the extent to which groundwater influences specific micro-catchments, particularly under low flows, the overall isotopic response is quite similar, especially when the catchment is wet and this responses can explain the isotope signatures observed in the stream. In future, more longitudinal studies of micro-catchments are needed to better explain the heterogeneity observed.

Key Words: riparian, wetlands, peat, isotopes, runoff, groundwater – surface water interactions.

1. Introduction

Riparian zones are defined as the areas fringing surface channel networks and thus, form an important interface between the terrestrial landscape and the riverscape. This interface is often a "hot spot" for water and nutrient exchange between aquatic and terrestrial systems, typically showing time variant dynamics of connectivity (Naiman and Decamps, 1997; Tetzlaff *et al.*, 2007a). The steep gradients in environmental conditions dictate that riparian zones are often distinct habitats in terms of biodiversity (Banner and MacKenzie, 1998; González *et al.*, 2016) and are usually, though not always, characterised by wetlands (Vidon, 2017). Such riparian wetlands (RW) often provide important ecosystem services; in headwater areas they may form a dominant source of stream flow generation (Bragg, 2002; Bullock and Acreman, 2003; Von Freyberg *et al.*, 2014), whilst in lowland areas they may provide storage zones for flood peak attenuation (Acreman and Holden, 2013). Headwaters in upland areas are of particular interest for runoff generation and contributions to downstream catchment-scale responses (Bragg, 2002; Partington *et al.*, 2013). In northern regions that have been subject to glaciation, RW often form in over-widened flat valley bottoms, and saturated areas with organic soils are sustained by seepage from deeper groundwater flow paths from upslope (e.g. Ala-aho et al., 2017), which also maintain base flows during dry seasons (Gilman, 1994; Sun *et al.*, 2016). During larger precipitation events, such RW can facilitate saturation excess overland flow (Penna *et al.*, 2015) and mediate the connectivity between catchment hillslopes and the stream network (Tetzlaff *et al.*, 2014; van Meerveld *et al.*, 2015; Sun *et al.*, 2016). Saturated RW have often been identified as being crucial for catchment scale storm runoff generation (e.g. Šanda et al., 2014). However, the small scale processes governing saturation and connectivity are rarely fully understood in detail. In particular, knowledge on how seasonal dynamics regulate non-linear spatio-temporal patterns of riparian saturation, and how this aggregates at larger scales is still missing.

In northern catchments, extensive histosols or peatlands in RWs are usually characterised by heterogeneous micro-topographical features known as hummocks (ridges) and hollows (depressions) (Kenkel, 1988; Chimner and Hart, 1996; Frei and Fleckenstein, 2014; Shi *et al.*, 2015). Some previous studies suggest higher groundwater levels in hummocks than in neighbouring hollows (Belyea and Clymo, 2001; Van der Ploeg *et al.*, 2012; Frei and Fleckenstein, 2014) and marked differences in vegetation cover, with the ecohydrology reflecting wetness (Kenkel, 1988; Malhotra *et al.*, 2016). However, other studies which focused more on the topographical patterning of peatlands and bogs as well as the connection to vegetation suggested a lower groundwater table in the hummocks than in the hollows (Rietkerk *et al.*, 2004; Eppinga *et al.*, 2008).

Modelling work by Frei et al*.*, (2010) suggested these micro-topographic variations play a key role in threshold-controlled “fill and spill” processes during storm events. Hollows would initially buffer rainfall input by providing transient storage, but with ongoing rainfall, neighbouring hollows fill and spill, developing connectivity. These form transient zero-order channels which can connect with the perennial channel network, causing a non-linear increase in storm runoff as overland flow increasingly dominates the hydrograph. Earlier modelling work (Esteves *et al.*, 2000; Fiedler and Ramirez, 2000) demonstrated that micro-topography affects the direction, depth and velocity of overland flow. Additionally, under homogenous infiltration rates, micro-topography is a major controlling factor for the development of local surface saturation and the subsequent connectivity of flow paths contributing to runoff generation (Qu and Duffy, 2007).

In addition to traditional hydrometric monitoring of groundwater levels and modelling of GW-SW interactions, environmental tracers can also provide insights into hydrological processes in RW (Tetzlaff *et al.*, 2014). In particular, tracers such as stable isotopes of water (deuterium (^{2}H) and 18-oxygen (^{18}O)) and geochemicals have proven utility for identifying water sources, tracing flow paths, estimating water ages and understanding saturation area dynamics (Neal *et al.*, 1997; McDonnell *et al.*, 1998; Kværner and Kløve, 2006; Tetzlaff and Soulsby, 2008; Barthold *et al.*, 2011; Lessels *et al.*, 2016; Tunaley *et al.*, 2017). In low-temperature environments, the isotopic composition of the natural waters are governed by physical phase changes (evaporation, condensation and melting) near and above the ground surface, as well as mixing at the surface and in the subsurface, making them very useful tracers (Leibundgut *et al.*, 2009). Sampling precipitation, groundwater and surface waters and analysis for tracers to identify sources and differentiate flow paths, as well as understanding the temporal dynamics of their contribution to runoff generation has become commonplace in catchment hydrology (Neal *et al.*, 1997; Kendall and McDonnell, 1998; Tetzlaff and Soulsby, 2008; Barthold *et al.*, 2011; Lessels *et al.*, 2016).

In recent years, a focal site for understanding runoff generation in RW has been the Bruntland Burn; a headwater catchment in the Scottish Highlands, which is characterised by a large peat-dominated

RW (Birkel *et al.*, 2011a, 2011b). Long-term and event-based hydrometric, stable isotope and modelling studies have shown that the RW in the Bruntland Burn is a “hot spot” area for runoff generation (Tetzlaff *et al.*, 2007b, 2008; Birkel *et al.*, 2011b; Blumstock *et al.*, 2015) and for mixing of different sources of soil water and groundwater (Soulsby *et al.*, 2015; Lessels *et al.*, 2016; van Huijgevoort *et al.*, 2016). During prolonging storm events, when the RW connects the hillslopes to the channel network, the runoff coefficient of the entire catchment can exceed 40% (Tetzlaff *et al.*, 2014) and even reach 80% in extreme cases (Soulsby *et al.*, 2017). However, despite extensive research on the general role of the RW, the localised small-scale GW-SW interactions involved in catchment runoff generation processes are still not very well understood. In this study, we investigate the spatial and temporal dynamics of GW-SW interactions in a RW at the scales of zero and 1st order micro-catchments and their associated micro-topography. We used hydrometric and tracer based-approaches to understand how groundwater and surface water interact at these small scales. The specific objectives are to:

1) Understand spatio-temporal dynamics in stable isotopes and hydrochemistry at the micro-catchment scale to understand GW-SW interactions and runoff generation.

2) Investigate how micro-topography (hollows, hummocks) reflect GW-SW interactions and runoff generation at larger scales.

Such process insights in such sensitive parts of headwater catchments is of vital importance for understanding their influence at the larger catchment scale and for evidence-based land management decisions (Soulsby *et al.*, 2017).

2. Study area

The study sites are located within the Bruntland Burn (BB) catchment, a 3.2 km^2 upland headwater in the Scottish Highlands (Figure 1). The BB is part of the Girnock Burn, a tributary to the river Dee (~2108 km²), the UK's largest catchment that is free of the influence of regulating reservoirs. The Dee is an important regional water resource, supplying drinking water for more than 300,000 people and sustaining an economically important Atlantic salmon (*Salma salar*) fishery (Tetzlaff *et al.*, 2012). The regional climate is marked by mild winters and cool summers; mean daily air temperature is 6°C, varying between 1 and 12°C in January and July, respectively. This reflects the maritime influence on the climate which is transitional between northern temperate and boreal. Annual average precipitation (P) is around 1100 mm a^{-1} (1993 – 2015 at Balmoral weather station, ca. 5 km west of the catchment) and is usually fairly evenly distributed throughout the year. Generally, half of annual P falls in frequent, but low intensity events (<10 mm d^{-1}). During winter, typically around 5% falls as snow, though this may exceed 10% during colder years. The mean annual potential evapotranspiration (ET) and runoff (R) are around 400 mm a^{-1} and 700 mm a^{-1}, respectively (Birkel *et al.*, 2011a). About 25 – 35% of the annual discharge is sustained by groundwater (Birkel *et al.*, 2011a, 2011b), though overland flow during precipitation events dominates the generation of the storm hydrograph resulting in a flashy flow regime (Soulsby *et al.*, 2015).

The landscape is heavily shaped by its glacial history, with a wide and flat valley bottom dominated by saturated organic-rich peat soils (histosols) forming RWs (Figure 1b). These are typically ~1.5 m deep and thin out to <0.5 m on the lower hillslopes where peaty gley soils predominate (Tetzlaff *et al.*, 2014). The peats in the low-lying RW are under quasi-permanently saturated conditions due their water-retentive nature and a perched water table that is usually within 0.2 m of the surface (Blumstock *et al.*, 2016). The RW is constantly supplied with groundwater seepage from steeper upslope areas (Tetzlaff *et al.*, 2014) and the extent of surface saturation – depending on antecedent wetness — varies between 2% to 40% of the total catchment (Birkel *et al.*, 2011b).

The steeper hillslopes have an average slope of around 14° and are dominated by podzolic soils. The higher altitude parts of the catchments, reaching 539 m a.s.l. (above sea level), are characterized by thin regosols and outcrops of exposed bedrock. The solid geology largely comprises granite and Si-rich and Ca-rich metasediments (Figure 1a) which are mostly covered by glacial drift deposits (which occupy about 70% of the catchment). The drift can reach up to 40 m in depth in the valley bottom (Soulsby *et al.*, 2007), where it typically has a silty-sand matrix with abundant larger clasts which thins out on the steeper hillslope (~5 m deep) into shallower, more permeable lateral moraines, and ice marginal deposits (Soulsby *et al.*, 2016). These drift deposits were identified as the main source of stored groundwater in the catchment (Soulsby *et al.*, 2015, 2016).

Whilst the peatlands in the RW are dominated by Spagnum mosses, together with grasses (e.g. *Molina caerulea*), the rest of the catchment is largely covered by heather shrubs (*Calluna vulgaris* and *Erica tetralix*) with tree cover restricted to areas of Scots pine (*Pinus sylvestris*) on some steep slopes or in fenced plantations. The trees are around 30 - 80 years old and range in height between 5 m and 20 m (Wang *et al.*, 2017). Total forest cover is about 10% with natural forest on the steep north-west hillslopes and in plantations near the outlet. Heavy grazing activities by a large red deer population prevents successful tree regeneration and preserves the dominance of the moorland vegetation.

Previous work has identified the RW in the BB as a key zone of runoff generation (e.g. Soulsby et al. 2016) — even after prolonged dry conditions (Tetzlaff *et al.*, 2014; Geris *et al.*, 2015). During precipitation events, the RW generates a considerable amount of saturation excess overland flow (e.g. Birkel, Tetzlaff, et al. 2011; Tetzlaff, Soulsby, Waldron, et al. 2007) channelling it directly into the stream through networks of perennial 1st order channels and ephemeral zero-order water tracks. Apart from directly generating runoff, during wetter conditions and as events increase in size, the RW increasingly connects the hillslopes to the stream network. These hillslopes deliver lateral flow path through macropores in the upper soil horizons and deeper groundwater seepage (Tetzlaff *et al.*, 2014; Geris *et al.*, 2015; Blumstock *et al.*, 2016). Within the RW, mixing of different source waters, i.e. soil water and groundwater, occurs with groundwater seepage increasingly dominant during dry periods (Lessels *et al.*, 2016).

3. Methods

Within the RW of the BB, small-scale dynamics of GW-SW interactions in selected micro-catchments were investigated from August 1st 2015 until August 31st 2016. This was undertaken within the wider context of the BB monitoring. An automatic weather station (Figure 1b) recorded precipitation with a temporal resolution of 15 min using a tipping bucket rain gauge connected to a CR800 Campbell logger (0.2 mm resolution). Stage height was recorded with the same temporal resolution at the BB catchment outlet (Figure 1b) using an Odyssey capacitance logger (0.8 mm resolution) and converted to discharge using a well-maintained rating curve. We also used data from two deeper wells drilled into the catchment drift; one in the riparian zone and one on the upper hillslope (Figure 1). These were screened at about 2m depth and water levels logged with divers (see Scheliga et al., (2017) for details).

In part of the RW, where most mixing of soil and groundwater takes place (Lessels *et al.*, 2016), we monitored the outlets of seven micro-catchments which are all within the quasi-permanently saturated area, but also drain steeper, upslope areas (Birkel *et al.*, 2011b). The seven micro-catchments belong to perennial 1st order channels on the south- (SF) and north-facing (NF) slopes with different source areas, flow regimes and landscape characteristics (Figure 1c, 2 and Table 1). The estimated surface drainage areas were derived from a high-resolution LiDAR survey, so they may not coincide with the groundwater catchment. Geospatial analyses used ArcGIS 10.3.1, R (version 4.3.1, (R Core Team, 2017)). The locations of channel networks were burned into the digital terrain model (DTM) for delineating the catchment areas. This was needed as small channels (<1 m widths) were not captured by the 1 x 1-m DTM. The DTM was cleaned of artificial "pits" before calculation of the flow direction (D8, (Jenson and Domingue, 1988)) and delineation of the catchment boundaries. The resulting areas of the micro-catchment range from 0.08 – 5.7 ha and the average slopes varied from 11 - 21°.

Rankers and podzols on the steeper hillslopes are the dominant soils in all micro-catchments. Under wet conditions, when the saturation area is at its highest extent (up to 40% of catchment area) (see Figure 2a), it closely matches the areas of peat and peaty gley soils in the micro-catchments. Under dry conditions, the micro-catchments of NFP II and SFP IV have a very small percentage of saturated area and - in the case of SFP V - none. The NFP II saturation area shrinks most dramatically, from 34% under wet condition to 1% under dry conditions. The SFP III saturation area does not change during different conditions, but it is the smallest under wet condition followed by the SFP IV (Table 1).

Both micro-catchments characterised by the north-facing perennial channels (NFP I & II) and one of the south- facing channels (SFP V) possess no tree cover. In contrast, in the micro-catchments SFP I, II, IV and SFP III the tree cover starts respectively around 290 m and 260 m a.s.l.. The small catchment area of the south-facing perennial channel V (SFP V) is the result of an old land rover track, diverting flow from a large portion of the original catchment area (Figure 2). Even though the micro-catchment surface areas of SFP II and III are also affected by this track, the catchment areas in the RW did not seem to be adversely affected.

We also investigated plot-scale micro-topography influences, at a location situated within the peatland of micro-catchment SFP II (Figure 2, Table 2). A NE-SW transect perpendicular to the direction of flow out of the micro-catchment was investigated (Figure 2c) across a series of hollows and hummocks which flow into the SFP II micro-catchment. *Molinia caerulea* and various *Sphagnum spp.* dominate the depressions, but heather (*Calluna vulgaris* and *Erica tetralix*) shrubs, with a Sphagnum understory characterise the elevated hummocky moraines. The micro-topography features provide a gradation of habitats for different *Sphagnum* species (Table S1). Whilst *Sphagnum fimbriatum, Sphagnum capillifolium* and *Sphagnum papillosum* were present across the transect, dominating the hollows, S. *capillifolium* and S. *papillosum* were more extensive on the hummocks below the heather.

We installed a shallow well cluster at the micro-topography site: five wells in each of the two dominant units (hummock and hollow) reaching 60 – 90 cm deep (Table 2). Wells were installed with a hand-auger and we used a white PVC (polyvinyl chloride) pipe with a 3.7 cm diameter as well casing. The casing was fully screened and fitted with the same type of Odyssey capacitance loggers used for stage height to monitor the shallow groundwater levels. The relative height difference of the ground surface between the locations of the micro-topography wells was measured using a robotic total station (Leica Geosystems TPS 1200) coupled with a 360° prism. The groundwater levels of the micro-topography wells were referenced to the ground surface height of the well at Hummock 2, because this had the highest ground surface elevation among the wells allowing direct comparison of the water table depths.

Precipitation and stream water samples were collected for isotope analysis on a daily basis at the BB outlet by two ISCO automated water samplers. A third auto-sampler was deployed in the perennial channels draining micro-catchment NFP I, also on a daily resolution. The remaining six perennial 1st-order channels draining the other micro-catchments were sampled at approximately biweekly resolution. In addition, we also sampled ephemeral water tracks on the south facing slope which became active during the wet winter period (Figure 3) and intended to repeat sampling during other wet periods, though they subsequently rarely flowed. The micro-topography wells were also sampled on seven occasions during the study period, mostly in 2016. Coordinates of the wells and sample locations were recorded with a GARMIN eTrex 10 handheld GPS (accuracy <15 m).

All water samples for isotope analysis were collected in 250 ml PVC bottles leaving no head space. Paraffin was added to auto-sampler bottles to prevent evaporative fractionation. After transport to the laboratory, samples were refrigerated until analysis. All water samples were analysed for their isotopic composition (δ^2H and δ^{18}O ratios) and the perennial water tracks samples from the micro-catchment outlets were also analysed for alkalinity. However, alkalinity samples from NFP I were only taken on the same biweekly resolution as the other six micro-catchments. A single set of samples from the micro-topography wells were also analysed for alkalinity. A Los Gatos IWA-35d-EP Laser Spectrometer (precision ±0.3‰ for δ^2H; ±0.1‰ δ^{18}O) was used to analyse the isotope ratios of the water samples. Every three samples, a standard was used to ensure accuracy. Samples which were flagged by the Post Analysis Software (Los Gatos) for organic contamination were filtered and re-analysed. The abundance ratio of heavy to light isotopes (^{2}H/^{1}H; ^{18}O/^{16}O) is reported in the δ-notion (in ‰) (Coplen, 2011) relative to the Vienna Standard Mean Ocean Water (VSMOW). Gran Alkalinity was determined according to Neal (2001) using acidimetric Gran titration to the endpoints pH 4.5, pH 4.0 and pH 3.0.

In dual-isotope space, the relationship between δ^2H and δ^{18}O in the precipitation signal (Dansgaard, 1964) provides a basis for identifying the extent to which water samples are affected by evaporative fractionation (Sprenger *et al.*, 2017). This relationship is described by the local meteoric water line (LWML). Deviations from this regression line (δ^2H = 7.6‰ × δ^{18}O + 4.7‰ for precipitation in the BB) indicates evaporation fractionation, if water samples plot below the LMWL. This deviation from the LMWL is caused by kinetic fractionation during evaporation (Craig *et al.*, 1963) and can be described by the line-condition-excess (lc-excess) defined by Landwehr and Coplen (2006):

$$lc - excess = \delta^2H - a \times \delta^{18}O - b \qquad \text{(Equation 1)}$$

Where *a* and *b* are the slope and intersect of the LMWL with a = 7.6‰ and b = 4.7‰, respectively for the BB.

We also selected eight storm events with contrasting antecedent wetness, duration and intensities to investigate the groundwater response in the micro-topography features using hysteresis loops for the discharge-groundwater table relationship. The hysteresis index (HI_{LL}) proposed by Lloyd et al. (2016) was used to characterize and compare the different storm events. The index was calculated from the average of the differences between the rising and falling limb of the GW level in the hysteresis loop at different percentages of the event discharge. The Differences were calculated for every 5% of the event discharge. This makes the HI_{LL} more suitable for complex loops and ensured a robust characterization of the respective storm events (Lloyd *et al.*, 2016). Discharge (Q) and the groundwater table (WT) for each well and storm event needed to be normalized to calculate HI_{LL}:

$$Normalized\ Q_i = \frac{Q_i - Q_{min}}{Q_{max} - Q_{min}} \qquad \text{(Equation 2),}$$

$$Normalized\ WT_i = \frac{WT_i - WT_{min}}{WT_{max} - WT_{min}} \qquad \text{(Equation 3).}$$

With Q_i and WT_i representing discharge and groundwater table at time step *i*, and $Q_{min/max}$ and $WT_{min/max}$ representing the respective extreme values for the event. HI_{LL} was calculated for each storm event loop as:

$$HI_{LL} = \frac{\sum (WT_{RL_{norm}} - WT_{FL_{norm}})_k}{n} \qquad \text{(Equation 4).}$$

With WT_{RL_norm} and WT_{FL_norm} representing the respective normalized (norm) groundwater level of the rising (RL) and falling limb (FL) at each discharge increment *k*. Index *k* starts at 0.05 (5% of event peak discharge) and increases in 0.05 steps until the maximum normalized storm discharge is reached. The sum is then divided by the total number of increments *n*, to determine the event average HI_{LL}. The HI_{LL} ranges from -1 to 1, the numeral represent the surface of the loops with small numbers indicating "narrow" and high numbers indicating "wide" loops. The sign of the HI_{LL} indicates the rotational direction of the loop, with a negative sign indicating anti-clockwise hysteresis and a positive sign clockwise hysteresis. The HI_{LL} for the more complex loop shapes (e.g. figure-8) was calculated from a weighted average, that was based the proportion the hysteresis loop rotated clockwise against the proportion it rotated anti-clockwise. If the hysteresis was predominantly rotating clockwise, the overall rotational direction of the event was classified as clockwise. The start of an event was the point when the discharge started to continuously increase, forming a clear rising limb. The end of the event was determined by either the discharge falling to at least 125% of the starting value or the start of a succeeding new discharge event.

4. Results

4.1 Hydroclimatic conditions during the study period

Generally, rainfall events during the study period were fairly evenly distributed and dominated by a high frequency of low intensity events <10 mm d^{-1} (Figure 3a). About half of the daily rainfall events were <1.5 mm in total. Very few events delivered rainfall totals >20 mm; these were mostly concentrated between December 2015 and January 2016, with a second wet period between June - July 2016. The December/January period was by far the most noteworthy, as it was marked by a succession of larger rainfall events which totalled 375.2 mm over just a few weeks. This unprecedented rainfall accounted for more than one-third of the annual average rainfall.

This high rainfall over a prolonged period resulted in high and sustained discharge peaks, exceeding 10 mm d^{-1} on 12 different days during December 2015 and January 2016 (Figure 3a). The highest peak discharge and precipitation amounts were recorded on the December 30th with 25.8 mm d^{-1} and 56.7 mm d^{-1}, respectively. The discharge response to lower intensity events for most of the remaining study period was more subdued, with pronounced high flows in response to a wet period in mid-June. Following this, the last month of the study period in summer 2016 was marked by prolonged low flows and the lowest recorded discharge of the period with 0.08 mm d^{-1} on August 27th. For the entire study period, Q_{95} and Q_5 were 0.11 and 6.24 mm d^{-1}, respectively.

The shallow groundwater levels in the RW were within ~25 cm of the soil surface throughout the year and highly responsive to each significant precipitation event with a rise in the water table and subsequent recession (Figure 3b). The riparian groundwater was artesian for several weeks in late December/early January and then again following the wet period in June. On the upper steeper hillslopes, groundwater fluctuations were much more pronounced. The water table was always within 110 cm of the soil surface, and only responded to larger rainfall events. In the December/January period the groundwater was very close to the soil surface; this is consistent with previous observations in wetter conditions, which showed that the high water table caused transmissivity feedback in the permeable organic soil horizons (~10 – 20 cm deep) with shallow lateral flow in the upper soil increasing the connectivity between the hillslopes and the drainage channel networks. Due to the freely draining nature of the subsoil in the hillslope podzols this high connectivity tends to be transient and declines rapidly following rainfall. However, these conditions were sustained for longer in the wet winter period.

4.2 Stable isotope and hydrochemistry dynamics of the micro-catchments

Figure 3c shows the daily δ^2H in precipitation, stream water and sampled water in NFP I, as well as the biweekly δ^2H dynamics of the other six monitored perennial micro-catchments. Isotopic variability in precipitation showed general seasonality with more frequent events enriched in δ^2H during the summer months and more depleted events during winter. However, in general the winter of 2015-16 was mild and precipitation was less depleted than usual. Nevertheless, strongly depleted precipitation events occurred in early December, and early and late January. The variation in stream water isotopes and the perennial micro-catchments showed similar seasonality but were greatly damped in comparison to precipitation (standard deviation of 24.6‰ and 2.4‰ for δ^2H in precipitation and stream water, respectively). Also, the extreme event in winter 2015/2016 caused a strong depletion in all surface water isotope samples. Most of the water from the perennial channels had a lower variability and standard deviation than stream water ranging from 1‰ to 2.4‰ for δ^2H (Table 3). Exceptions were NFP II and SFP I, which showed the highest isotopic variability with standard deviations of 3.8‰ and 4‰ for δ^2H, respectively; this mainly reflected the elevated summer levels (Figure 3c). Notably, these two micro-catchments do not originate from a spring or a single pool like the others (Table 1). NFP II has a large seepage area as its source and SFP I has an extensive network of pools.

This damping relative to precipitation is evident when samples are plotted in dual isotopes space (Figure 4a). The channels draining the perennial micro-catchments show more variability than stream water leaving the BB and the boxplots for δ^2H and δ^{18}O (Figure 4b and c) show that on average they tend to be more depleted, though they also have more enriched samples (Table 3). But in general, they occupy the same space with a similar regression line. The lower regression slope relative to precipitation – where the LMWL plots close to the global meteoric water line (GMWL) - is indicative of evaporative fractionation in more enriched summer samples (see equations in Table S2). The prevailing dry conditions following the January/December wet periods, dictated that the ephemeral water tracks could only all be sampled in January 2016, these mostly plotted above of the LMWL and showed limited signs of evaporative fractionation, though a few samples collected at the few flowing sites in the summer plotted below the line.

Figure 5 shows the samples of the individual micro-catchments separately and highlights more of the heterogeneity and spatial variability. All of the ephemeral water tracks are also shown. NFP II and SFP I showed the largest isotopic ranges while NFP I, SFP III and IV had the narrowest. Most of the regression lines of the micro-catchments plotted close to that of the stream water – though SFP IV had a notably less steep slope. Only a limited numbers of samples plotted distinctly below the LMWL suggesting evidence of evaporative fractionation. These samples occurred mainly during autumn 2015 (samples of NFP II, SPF I and SPF V) and during spring 2016 (samples from SPF I and the ephemeral water tracks (EWTs)) and during early-summer 2016 (samples from the stream and the EWT).

Figure 6 pools all samples of the perennial micro-catchments as a time series of sampling dates to reveal the seasonal patterns more clearly. For most of the study period, the stable isotope signals for individual sampling days exhibited marked spatial variability evident in the large ranges. However, during and after the large storms in December/January spatial variability was much more compressed in the wetter conditions, with around ~5‰ difference between the δ^2H values which were all low. Greatest variability in δ^2H was evident during the summer and autumn months when flows were lowest with average differences in δ^2H values of ~8 and ~7‰, respectively consistent with the effects of summer rainfall and evaporative fractionation at some sites (Figure 6b), although these differences again narrowed in the wet June period.

Using the lc-excess of samples provides further process insight in relation to evaporative fractionation. The long-term average lc-excess of precipitation is around zero, though individual samples varied temporally with positive and negative values evident throughout the year, indicating different air mass sources and recycling of atmospheric moisture (Figure 3d). The lc-excess in the stream or the channels of the micro-catchments were much more stable, with values rarely negative, and uncorrelated with the lc-excess of rainfall. Periods with negative lc-excess were most common in summer and autumn 2015, and again in summer 2016, as is evident in the averaged values of the perennial micro-catchments in Figure 6c. The spatial variability of lc-excess across the PWTs micro-catchments was limited during the winter and throughout the spring (Figure 6c). In contrast, summer and autumn showed larger spatial variability in lc-excess. The highest average difference was seen during summer (~6‰). For example, in October 2015, samples from SFP V, SFP I and NFP II showed clear evaporation fractionation signal with lower lc-excess values (Figure 3d). During relatively dry periods in February 2016 and June 2016, NPF I and SFP I showed also rather low lc-excess values close to -5‰, respectively, showing some local hotspots for fractionation processes. These sites are all characterised by sources of diffuse seepage or pool networks where opportunities for evaporation occur as a result of low long residence times.

Gran alkalinities in the perennial channels generally varied with discharge, with all sites being <50 µEq l^{-1} in the wet January periods. All sites exceeded 100 µEq l^{-1} under low flow conditions, though variability under dry conditions was most pronounced (Figure 3e and 6d). The dominance of more acidic, soil-derived overland flow when wet, and the dominance of deeper groundwater sources when dry explains this variation. Most sites showed limited temporal variability for much of the year, with standard deviations mostly ranging between 20 µEq l^{-1} and ~50 µEq l^{-1} (Table 3). However, similar to the isotope signatures, SFP I and NFP II displayed the highest standard deviations with 113 and 65 µEq l^{-1}, respectively. SFP I generally had the highest alkalinity of all the micro-catchments in its perennial channel. In contrast, SFP III generally had the lowest alkalinity with an average of 80 µEq l^{-1}.

The first, and only complete sampling of the EWTs was in early January 2016 at the time of peak wetness (See supplementary material Figure S1). On January 7th and 8th 2016, all sampled EWTs were depleted similar to stream water (cf Figure 3c). Such depleted signatures continued for the remaining active south facing ephemeral water tracks (SFE 1, SFE 3, SFE 10), except SFE 11 which started to have a more enriched isotopic signal after April 2016. These more enriched samples had persistently low lc-excess values (Figure S1), and they are the EWT samples, which plotted distinctively below the LMWL (Figures 4 and 5) showing evidence of evaporative fractionation. All the EWT samples had low alkalinity values on the January 7th 2016 ranging between 21.3 – 60 µEq l^{-1} consistent with soil-derived runoff generation (Figure 7 d). The following day, only SFE 7 and SFE 11 remained actively flowing, showing a marked change with the SFE 7 having the lowest alkalinity value from all EWTs (21.3 µEq l^{-1}) and the highest value on January 8th with 238.9 µEq l^{-1} as groundwater influence returned. Such groundwater dominance was evident when EWTs were flowing in spring and summer and were all >100 µEq l^{-1}.

4.3 Influence of Micro-topography on groundwater

In all wells of the micro-topography cluster, the shallow groundwater levels responded rapidly to almost every precipitation event (Figure 7). In general, the water table was around 10 cm shallower in the hollows, than the adjacent hummock, though Hollow IV and Hummock 4 were an exception. The differences between hollows and hummocks was greatest during drier periods. All micro-topography wells recorded their highest water levels during the larger storm events in late-December 2015 / early-January 2016 and were again high in the large rainfall event (>40 mm) in late-June 2016. Comparing the micro-topography wells along the general local slope (going NE to SW) shows the highly localised spatial heterogeneity of the overall water table (Figure 7d). This variability of the groundwater table was not limited to specific micro-topography features or locations along the local slope as it is also influenced by water fluxes from upslope. However, in general, lower variability was evident in the hollows and greater variability under the hummock. The lowest and highest standard deviations in groundwater levels both occurred in the hollows with 0.6 cm and 3.5 cm in Hollow I and Hollow III, respectively (Table 4). For the other hollows, standard deviations ranged between 1.3 cm and 2.1 cm. Most of the hummocks had standard deviations above 2 cm (Table 4).

Most stable isotope samples from the micro-topography wells plot slightly above the long-term LMWL (Figure 8) though this may reflect the spring/summer bias of the sampling. Of the four regression lines that had slopes lower than that of stream water, three were in hollows (I, IV and V) and the fourth was from Hummock 5, though overall there was no systematic differences between hummocks and hollows (see equations in Table S2). On average, Hummock 3 had the most enriched samples with mean δ^2H -54.3‰ and Hollow I had the most depleted samples with mean δ^2H -60.2‰ (Table 5). The lowest variability in isotopic composition was in Hollows V and I and Hummock 4 with standard deviations of 0.6‰, 0.8‰ and 1.1‰, respectively. All hummocks had mean lc-excess values of 1‰; in the hollows the mean lc-excess values ranged between 0 – 3‰ (Table 5). Most of the micro-topography wells showed signs of evaporative fraction, which was more pronounced in the hollows (see regression slopes in Table S2). Interestingly there was a significant ($p<0.05$) positive correlation between indices of water table variability and the variability in isotope composition, with the relationship clearest in the hollows (Figure 9a). This is consistent with greater influxes of water from upslope varying the water levels and the isotopic composition, whilst less marked water level variation was characterised by more stable isotope composition. The micro-topography wells were also sampled for alkalinity once, on the November 27th 2016. In contrast to the isotopes, alkalinity values showed substantial differences ranging from -6.4 µEq l^{-1} to 294 µEq l^{-1} in the hollows, and between 31.2 and 247.1 µEq l^{-1} in the hummocks. However, the alkalinity of individual wells was negatively and significantly ($p<0.05$) correlated with variability in the water-table and isotope variability (Figure 9). This is consistent with higher alkalinity groundwater dominating wells which have more stable hydraulics and isotope composition.

To better understand the relationships between stream discharge and groundwater levels monitored in the hollows and hummocks, we also investigated hysteresis loops. Figure 10 shows two representative events (Event 1 and 5 in Figure 7) out of eight investigated (Table 6). Almost all hysteresis loops are narrow and have a clockwise direction, meaning that groundwater levels responded before the stream, except for seven occasions in three different wells but all in the hollows (I, II and III). Loops rarely displayed a figure-eight or more complex pattern. In fact, all complex loop patterns occurred during event 6 (Table 7). This event occurred over three days with larger events (17 mm, >40 mm and ~10 mm) which triggered a response in the stream and the wells (Figure 7). The largest change in groundwater levels during an event was either during Event 1 (Hollow II, Hollow V and Hummock 5) or during Event 6 (all other wells). Amongst the hollows, Hollow III had on average the highest changes in groundwater level during events; and had the highest rise during a single event (E6) with 14.9 cm. Other hollows had on average a rise of 2.3 cm during events, with Hollow I recording usually the lowest changes (Table 6). Overall, during the investigated events the groundwater levels inside the hummocks rose on average roughly 60% (~2.4 cm) higher than inside the hollows.

5. Discussion

Groundwater dynamics in micro-catchments

Our results help to understand the spatio-temporal influence of GW-SW interactions in micro-catchments. In this regard, the data have shown the spatial heterogeneity of how the rainfall-runoff response of the Bruntland Burn catchment reflects variation in the relative importance of groundwater exfiltration, soil water storage and mixing of new rainfall in the micro-catchments driven by dynamics in the micro-topographic features of the RW. The isotopes and geochemistry have shown some heterogeneity but, overall, the responses were rather similar. Some micro-catchments were characterised by a stronger groundwater imprint, with more depleted and stable isotope values, higher lc-excess and more stable alkalinities. Thus, it is significant that the micro-catchments NFP I, SFP II and SFP III which have such conditions, are characterised by springs or upwelling groundwater in pools (Table 1, 3). Conversely, diffuse seepage-fed micro-catchments (NFP II, SFP I) tended to be more variable and mixed, and showed more evidence of evaporative fractionation. These results confirm findings by Lessels et al*. (*2016) identifying the RW as the key mixing area of different source waters, though this is mediated in the micro-catchments of zero-order channels. Such fine-scale heterogeneity would be impossible to detect by only sampling at the catchment outlet emphasising the importance of spatial distributed sampling of key locations to better understand heterogeneities in dominant runoff generation processes (Jencso et al*.*, 2010).

This spatial variation was, however, mediated by the influence of antecedent wetness and characteristics of hydrological events. Thus, spatial heterogeneity of tracer signals was less clear during and after the large precipitation events in December 2015 and January 2016, when the catchment was wet and highly connected. During such wet periods, relative groundwater contributions to runoff generation are reduced and surface runoff generation through saturation overland flow becomes the dominant process. The subsequent mixing with large water inputs homogenised the tracer signals across the RW. The daily sampling of stream water and of NFP I revealed substantially depleted signals early-December 2015 and late-January 2016, which coincided with depleted precipitation input signals. This indicates an increased contribution of younger water from saturation excess overland flow (McGlynn and McDonnell, 2003). These short-term dynamics were not picked-up with the bi-weekly sampling of the perennial channels, underlining the importance of high resolution sampling. The dominance of surface runoff in wet conditions was also reflected in the alkalinity values, which were low and almost uniform across the sampled sites. Even after this wetter period, the isotopic values across the micro-catchments remained quite uniform with δ^2H values close to -59‰ from late-January until late-April, 2016, indicating displacement of well-mixed soil water storage across the RW following the large water inputs, despite the increasingly drier conditions (Soulsby et al., 2015). In the summer as the catchment dried, isotopic heterogeneity increased and fractionation effects were evident.

This dominant, but time-variant, influence of RW is consistent with the findings of other studies in northern/upland environments where organic soils are important. For example, Correa et al., (2017) in the upland Zhurucay catchment in Ecuador (7.6 km^2) identified water from riparian zone as the highest contributor to runoff throughout the year; event water flows above the saturated histosol in riparian zone and feeds directly in to the stream. Similarly, Peralta-Tapia et al. (2015) examined isotopic tracers in 78 sub-catchments of the Krycklan watershed in Sweden at scales from 0.12 - 68 km^2. The isotopic composition of smaller catchments which had greater coverage of wetlands (up to 40%) showed the influence of both summer and autumn precipitation in younger soil waters influencing runoff, while larger sub-catchments had compositions similar to deeper groundwater. The contributions of deeper groundwater to annual runoff increased with catchment area from ~20% in small headwater sub-catchments to 70 - 80% in large catchments (>10.6 km^2). At larger scales, Devito et al. (2017), working in meso-scale catchments in low-relief in the Boreal Plain of Canada at scales from 50 – 5.000 km^2, showed how peatlands were the major source of runoff. Penna et al., 2016 also identified the importance of wetness on temporal dynamics of runoff generation. Working in the Bridge Creek Catchment (0.14 km^2) in Italian Alps, they showed that during dry conditions saturation excess overland flow and direct channel precipitation dominated runoff processes; whilst during wet conditions riparian groundwater contributions increased.

The importance of the riparian areas for mixing different source waters and runoff generation has also been observed in other geographical settings and shown how a connected RW can control the spatial and temporal heterogeneity of the isotopic composition of the stream water. For example, Fischer et al., (2015) investigated micro-catchments in a Swiss pre-alpine headwater catchment. Base flows were sustained by deeper groundwater and showed little fine scale spatial heterogeneity. However, the temporal variability in deuterium was marked as wetland areas inside the micro-catchment connected to the stream network. Similarly, Klaus et al., (2015) investigated the runoff dynamics from RW in three adjacent small, lowland headwater catchments in the Upper Atlantic Costal Plan in USA. The RWs exerted a strong control over the isotopic composition of the stream. As stream water moves slowly through the RW, evaporative fraction processes strongly influence the isotopic composition of the stream water.

Likewise, larger precipitation events not only exert an event-based control on RW, but also a longer lasting regulation of runoff generation and stream isotope composition which exceeds the event duration. The influence of event size and antecedent conditions on mediating the effects of runoff generation and stream isotope composition have been reported for large events. For example, McGlynn et al., (2004) investigated the scale effect on runoff responses for two events from different sized catchments (0.26 - 0.8 km^2) inside the Maimai catchment in New Zealand. Both events, (of 27 mm and 70 mm) diluted tracer signals with the impact greatest in the large event and was most evident at larger scales. This is similar to what Didszun and Uhlenbrook (2008) reported, when also investigating the scale effect of runoff processes in different sized nested catchments (0.015 – 258 km^2) inside the Dreisam catchment in Germany. They also observed increasingly homogenous tracer signatures during large events across the micro- and smaller catchment (1 – 40 km^2) and suggesting the prevalence of similar dominant runoff processes at all scales.

Groundwater dynamics inside the micro-topography features

In terms of the processes underpinning runoff generation in the micro-catchments, the water table and tracer responses of the hollows and hummocks also revealed some heterogeneity. In general, the hollows had shallower groundwater and the isotopic composition tended to be more depleted and more prone to fractionation. However, the groundwater variability was also generally more marked in the hummocks. It is significant that the relationships in Figure 9 show that the wells with greatest groundwater variability tended to have the most variable isotope signatures and lowest alkalinity. Conversely, the less variable groundwater fluctuations which tended to be the hollows had the most consistent isotope signals and highest alkalinity. This suggests a more stable, persistent groundwater influence and efficient flow system for evacuating excess water. In contrast, the more variable sites (mainly the hummocks) were generally drier but could be inundated in the largest events from upslope drainage. In this regard, similar hydraulic responses were reflected in the hollows and hummocks showing similar groundwater level hysteresis relative to stream flow, being dominated by clockwise loops indicating groundwater peaking before stream flow. This was occasionally reversed in some hollows which may be indicative of groundwater influxes from upslope continuing after the event.

The role of the micro-topography was similar to that identified by Frei et al., (2010) who modelled a 10 m x 20 m part of the RW in the Lehstenbach catchment, Germany. They showed the micro-topography efficiently buffered rainfall; with modelling reproducing a fill and spill mechanism in the hollows during intensive rainfall which resulted in a shift from subsurface flow dominance to surface flow dominance. Moreover, they found that for steady rain input a stepwise development of the surface flow network occurred; whilst for variable rain input the surface networks would dynamically expand and shrink. Later work by Frei and Fleckenstein (2014) assumed higher water tables in hummocks resulted in shallow groundwater flow towards the hollows. However, others have reported more complex conditions with higher water tables in the hollows and shallow groundwater flows towards the hummocks. Malhotra et al., (2016) for example, investigating the relationship between groundwater levels and micro-topography features in a wetland at Mer Bleue, Canada, found that the water table was generally higher inside the hollows compared to the hummocks. In some locations there was a strong relationship between groundwater table and its micro-topography features, whilst in others there was not. Eppinga et al., (2008) also found generally higher groundwater levels inside hollows. However, they also reported higher nutrient concentrations inside the hummocks suggesting that the nutrients are transported from the hollows to the hummocks. Given the dynamic nature of peatland surfaces and the diversity of peatland sites, such variation is not surprising and underlines the need for more small scale investigations, nested within larger catchment studies. In this regard, our work has raised new questions, particularly the need to extend micro-topography studies to better understand the longitudinal influence of upslope processes.

Conclusion

We used hydrometric monitoring, isotopes and other tracers to understand runoff generation processes in a large valley bottom riparian wetland in a catchment in the Scottish Highlands. Whilst the rainfall-runoff response of micro-catchments in the wetland, and associated hummock and hollows systems, showed some heterogeneity, they generally exhibited similar behaviour in terms of being mixing zones for groundwater seepage, with resident soil water and incoming precipitation. Spatial and temporal differences observed in the micro-catchments and in the micro-topography features reflected the differing relative influence of older groundwater (which tended to be isotopically depleted, more constant and enriched in alkalinity) and younger soil waters which had the isotopic imprint of recent precipitation, low alkalinity and occasionally showed evidence of evaporative fractionation. “Fill-and-spill” processes in the hollow and hummock systems occur during precipitation events and drive the increased connectivity between the riparian wetlands and river channel networks. More detailed longitudinal hydrometric and isotopic studies are needed along the permanent channels and ephemeral water tracks to better understand the evolution of these processes and try to integrate them in catchment models.

Acknowledgements

We would like to thank the European Research Council (ERC, project GA 335910 VeWa) for funding.

Tables:

Table 1: Characteristics of the north (NFP) and south facing perennial micro-catchments (SFP), estimates of saturation extent are based on the empirical model of Birkel *et al.* 2011b.

ID	**Catchment area**	**Major source of water**	**Description of flow characteristics**	**Peat**	**Peaty Gley**	**Peaty podzol, ranker and Brown ranker**	**Saturation extent - dry**	**Saturation extent - wet**	**Slope**	**Tree cover**
	[ha]			**[% of Micro-catchment area]**					**[°]**	
NFP I	3.1	Spring	All year long very strong flow	18	15	67	26	34	11	no trees
NFP II	5.3	Large seepage area	Mostly strong flow, little flow during dryer conditions	2	28	70	1	34	11	no trees
SFP I	5.7	Network of connected pools	Mostly strong flow all year, weaker during dry condition	23	-	77	15	19	17	> 293 m a.s.l.
SFP II	3.8	Spring	Strong flow all year	15	-	85	9	12	21	> 293 m a.s.l.
SFP III	3	Spring	Strong flow all year	4	-	96	4	4	23	> 260 m a.s.l.
SFP IV	2.8	Pool	Mostly strong flow all year, weaker during dry conditiond	8	-	92	1	5	21	> 293 m a.s.l.
SFP V	0.08*	Spring	Very little flow all year	38	-	62	0	13	12	no trees

* Catchment area cut-off by a land rover track

Table 2: Characteristics of the wells of the micro-topography survey, all on peat soil and above granite and the drift deposit. All wells are around 255 m a.s.l. and all fully screened; the study site is located within the micro -catchment SFP II.

ID	Depth [cm]	Distance to Stream [m]	Distance to Outlet [m]	Slope [°]
Hollow I	50	110	723	6.3
Hollow II	60	109	730	4.3
Hollow III	60	110	733	3.3
Hollow IV	60	100	738	3.7
Hollow V	60	93	741	1.1
Hummock 1	60	112	727	10.2
Hummock 2	90	109	731	3.8
Hummock 3	90	97	738	2.3
Hummock 4	80	93	740	2.2
Hummock 5	90	92	744	1.1

Table 3: Summary statistics (mean, median, standard deviation, standard error) for δ^2H, $\delta^{18}O$ and alkalinity of the perennial channels of north and south facing micro-catchments.

ID	Number of samples	δ^2H [‰]				$\delta^{18}O$ [‰]				lc-excess [‰]				Alkalinity [µEq. l^{-1}]			
		Mean	Median	Std. dev.	Std. error	Mean	Median	Std. dev.	Std. error	Mean	Median	Std. dev.	Std. error	Mean	Median	Std. dev.	Std. error
Precipitation	210	-56.3	-52.2	24.6	1.7	-7.8	-7.3	3.1	0.2	-1	-2	5	0	-	-	-	
Stream	397	-57.8	-57.5	2.4	0.1	-8.5	-8.5	0.4	0	2	2	2	0	-	-	-	
NFP I_{Daily}	276	-59.7	-59.7	2.2	0.1	-8.8	-8.9	0.4	0	3	3	2	0	-	-	-	
NFP I	31	-60.7	-60.3	1.3	0.2	-9	-9	0.3	0.1	3	3	2	0	175.5	183.3	50.3	8.6
NFP II	35	-57.3	-56.4	3.8	0.6	-8.4	-8.4	0.6	0.1	2	2	2	0	101.2	95.4	65.6	11.3
SFP I	35	-55.8	-55.7	4	0.7	-8	-8	0.8	0.1	0	0	3	1	255.5	267.1	113.2	19.4
SFP II	35	-57.9	-57.7	2.1	0.4	-8.4	-8.4	0.4	0.1	1	1	1	1	137.4	144.1	37.1	6.4
SFP III	34	-59.5	-59.5	1.3	0.2	-8.8	-8.8	0.3	0.1	2	3	1	0	79.7	77.8	20.7	3.6
SFP IV	34	-60	-60	1	0.2	-8.9	-8.9	0.3	0.1	3	3	1	0	96.8	100	26.8	4.6
SFP V	34	-57.6	-58	2.4	0.4	-8.3	-8.4	0.5	0.1	1	1	2	0	100.5	98.7	35.6	6.1

Table 4: Statistics of the shallow groundwater wells inside the micro-topography features showing the minimum, maximum, mean, standard deviation, topography wetness index and the dominant moss vegetation. The groundwater levels are in reference to the ground surface at well Hummock 2, which had the highest local elevation.

ID	Groundwater level					TWI	Dominant species in vicinity
	Min	Max	Mean	Median	Std. dev		
	[cm]	[cm]	[cm]	[cm]	[cm]	[-]	Sphagnum (S.) & Warnstorfia (W.)
Hollow I	-33.8	-27.2	-31	-31.1	1.1	-33.8	S. capillifolium
Hollow II	-27.8	-12.4	-18	-17.7	2.3	-27.8	S. fimbriatum, S. capillifolium, S. papillosum
Hollow III	-37.3	-16.5	-27.5	-28	3.8	-37.3	S. fimbriatum
Hollow IV	-45.5	-36	-40.9	-41	1.9	-45.5	S. fimbriatum
Hollow V	-34.1	-25.5	-28.7	-28.4	1.3	-34.1	S. fimbriatum
Hummock 1	-45	-31	-38.2	-38	2.6	-45	S. papillosum
Hummock 2	-35.5	-11.2	-30.1	-30.6	2.9	-35.5	S. papillosum
Hummock 3	-50.1	-28.4	-45.2	-45.6	2.5	-50.1	S. capillifolium
Hummock 4	-42.2	-31.4	-36.9	-37.1	1.5	-42.2	S. papillosum
Hummock 5	-38.2	-17.7	-30.7	-30.9	2.9	-38.2	W. sarmentosa

Table 5: Summary statistics (mean, median, standard deviation & standard error) for δ²H and δ¹⁸O for the micro topography wells.

ID	Number of samples	δ²H [‰]				δ¹⁸O [‰]				lc-excess [‰]				Alkalinity [µEq l⁻¹]
		Mean	Median	Std. dev.	Std. error	Mean	Median	Std. dev.	Std. error	Mean	Median	Std. dev.	Std. error	sampled once
Precipitation	210	-56.3	-52.2	24.6	1.7	-7.8	-7.3	3.1	0.2	-1	-2	5	0	-
Stream	397	-57.8	-57.5	2.4	0.1	-8.5	-8.5	0.4	0	2	2	2	0	-
Hollow I	7	-60.2	-60.4	0.8	0.3	-9	-9	0.1	0	3	3	1	0	141.7
Hollow II	7	-54.5	-54.9	4.1	1.5	-7.9	-7.9	0.7	0.3	0	0	2	1	3.7
Hollow III	7	-55.7	-56.5	4	1.5	-8.2	-8.4	0.6	0.2	2	2	1	0	-6.4
Hollow IV	7	-57.6	-57.9	1.4	0.5	-8.5	-8.5	0.3	0.1	2	2	2	1	231
Hollow V	7	-56.3	-56.5	0.6	0.2	-8.2	-8.2	0.3	0.1	1	1	2	1	293.6
Hummock 1	7	-57.6	-57	2.2	0.8	-8.3	-8.4	0.4	0.2	1	1	1	0	31.2
Hummock 2	7	-56.5	-57.3	1.9	0.7	-8.3	-8.3	0.3	0.1	1	2	1	0	32.5
Hummock 3	7	-54.3	-55.6	2.6	1.0	-7.96	-8	0.4	0.2	1	0	1	0	156.6
Hummock 4	7	-55.6	-55.6	1.1	0.4	-8	-8.1	0.2	0.1	1	0	1	0	247.1
Hummock 5	7	-58.2	-58.6	3.4	1.3	-8.3	-8.3	0.6	0.2	1	1	2	1	118.1

Table 6: Summary statistics for the eight hysteresis events showing the pre-event discharge (Q_{pre}), the peak discharge of the event (Q_{max}), total amount of Rain during the event (P_{total}), the amount of rain seven days prior to the event (P_7), the pre-event groundwater level in the wells (pre), the highest recorded water table during the event (max) and the groundwater table difference (Δ = max- pre), the groundwater level is in respect to the ground surface at well Hummock 2, bold values indicate highest value across the eight events.

Event	Start	End	Q pre [m^3/s]	Q max [m^3/s]	P total [mm]	P 7 [mm]	Hollow I			Hollow II			Hollow III			Hollow IV			Hollow V		
							pre [cm]	max [cm]	Δ	pre [cm]	max [cm]	Δ	pre [cm]	max [cm]	Δ	pre [cm]	max [cm]	Δ	pre [cm]	max [cm]	Δ
1	24/10/15	27/10/15	0.03	0.18	13.1	2.5	-	-	-	-24.4	-17.1	**7.3**	-32.5	-21.5	11	-43.3	-39.6	3.7	-32.2	-29.1	**3.1**
2	15/12/15	19/12/15	**0.08**	0.39	16.4	19.5	-	-	-	-17.5	-15.4	2.1	-27.6	-19.4	8.2	-39.5	-38.3	1.2	-28.1	-27.1	1
3	22/01/16	24/01/16	0.04	0.17	5.8	1.8	-31.6	-31.5	0.1	-17.5	-16	1.5	-28.4	-22	6.4	-39.5	-37.9	1.6	-27.8	-27.2	0.6
4	16/02/16	19/02/16	0.03	0.31	8.8	4.5	-31.6	-31	0.6	-17.5	-15.1	2.4	-26.5	-18.7	7.8	-40.7	-38.4	2.3	-28.3	-27.1	1.2
5	22/05/16	25/05/16	0.01	0.23	16.3	13.5	-31.7	-30.8	0.9	-18.1	-13.3	4.8	-29.4	-18.7	10.7	-42.4	-38.7	3.7	-28	**-25.6**	2.4
6	14/06/16	23/06/16	0.01	**0.68**	**70.2**	15.2	-32.8	**-27.2**	**5.6**	-17.5	**-12.9**	4.6	-31.9	**-17**	**14.9**	-42.3	-37.5	**4.8**	-28.9	-25.9	3
7	11/07/16	12/07/16	0.03	0.41	9.9	23.3	**-30.1**	-29.6	0.5	**-15.2**	-13.2	2	**-26.4**	-20.3	6.1	-39.5	-37.3	2.2	**-27.7**	-26.3	1.4
8	24/07/16	25/07/16	0.01	0.11	11.7	**27.2**	-29.2	-29	0.2	-16.4	-14.5	1.9	-28.1	-22.2	5.9	**-39.3**	**-37.2**	2.1	-27.9	-26.6	1.3

Event	Start	End	Q pre [m^3/s]	Q max [m^3/s]	P total [mm]	P 7 [mm]	Hummock 1			Hummock 2			Hummock 3			Hummock 4			Hummock 5		
							pre [cm]	max [cm]	Δ	pre [cm]	max [cm]	Δ	pre [cm]	max [cm]	Δ	pre [cm]	max [cm]	Δ	pre [cm]	max [cm]	Δ
1	24/10/15	27/10/15	0.03	0.18	13.1	2.5	-44	-37.6	6.4	-32.7	-24.6	8.1	-48.6	-40.7	7.9	-40.2	-37.3	2.9	-36.9	-26.6	**10.3**
2	15/12/15	19/12/15	**0.08**	0.39	16.4	19.5	-38.4	-33.6	4.8	-31.7	-20.6	11.1	-45	-39	6	-36.8	-35.4	1.4	-30.8	-25	5.8
3	22/01/16	24/01/16	0.04	0.17	5.8	1.8	-37.6	-34.6	3	-32	-23.8	8.2	-45.4	-42.5	2.9	-36.5	-35.9	0.6	-31.2	-28	3.2
4	16/02/16	19/02/16	0.03	0.31	8.8	4.5	-37.6	-32.8	4.8	-31.9	-19.9	12	-45.6	-41.1	4.5	-36.8	-35.8	1	-29.3	-23.9	5.4
5	22/05/16	25/05/16	0.01	0.23	16.3	13.5	-39	-33.5	5.5	-31.9	-21.2	10.7	-45.9	-35.3	10.6	-37	-34.9	2.1	-29.2	-20.4	8.8
6	14/06/16	23/06/16	0.01	**0.68**	**70.2**	15.2	-40.6	**-32.5**	**8.1**	-30.7	**-14.6**	**16.1**	-46.3	**-32**	**14.3**	-36.1	-33	**3.1**	-29.3	**-19.3**	10
7	11/07/16	12/07/16	0.03	0.41	9.9	23.3	-36.4	-33.8	2.6	**-27.4**	-22.5	4.9	-44	-37.8	6.2	-33.9	-32.2	1.7	-24.8	-19.5	5.3
8	24/07/16	25/07/16	0.01	0.11	11.7	**27.2**	**-35.9**	-33.6	2.3	-29.3	-26.6	2.7	**-43.5**	-38.1	5.4	**-33.3**	**-31.6**	1.7	**-24.5**	-19.5	5

Table 7: Hysteresis Index (HI_{LL}) values for the 8 different events (E1-8); negative values indicate anticlockwise and positive values clockwise behaviour; the values can range from -1 to 1 and large values indicate the "fatness" of simple loops; Dir = hysteresis direction, A = anti-clockwise, C = clockwise, [8] = indicating a figure-of-eight shape and ** = indicating a more complex shape.

Event	Hollow I		Hollow II		Hollow III		Hollow IV		Hollow V		Hummock 1		Hummock 2		Hummock 3		Hummock 4		Hummock 5	
	HI_{LL} [-]	Dir	HI_{LL} [-]	Dir	HI_{LL} [-]	Dir	HI_{LL} [-]	Dir	HI_{LL} [-]	Dir	HI_{LL} [-]	Dir	HI_{LL} [-]	Dir	HI_{LL} [-]	Dir	HI_{LL} [-]	Dir	HI_{LL} [-]	Dir
1	-	-	0.03	C	0.09	C	0.5	C	0	C	0.2	C	0.37	C	0.29	C	0.11	C	0.5	C
2	-	-	0.57	C[8]	-0.02	A	0.2	C	0	C	0.1	C[8]	0.39	C	0.24	C	0.44	C	0.3	C
3	0.37	C	0.49	C	-0.17	A	0.3	C	1	C	0.1	C	0.13	C[8]	0.19	C	0.58	C	0.2	C
4	-0.3	A	0.61	C	0.09	C	0.2	C	0	C	0.5	C	0.54	C	0.38	C	0.46	C	0.5	C
5	-0.5	A	0.27	C	0.19	C	0.1	C	0	C	0.1	C	0.35	C	0.47	C	0.43	C	0.5	C
6	-0.5	A	0.27	C	0.19	C	0.1	C**	0	C**	0.1	C**	0.35	C**	0.47	C**	0.43	C**	0.5	C**
7	0.31	C	0.35	C	0.28	C	-0.1	A[8]	1	C	0.5	C	0.36	C	0.54	C	0.38	C	0.5	C
8	0.32	C	0.4	C	0.15	C[8]	-0.2	A[8]	0	C	0.5	C	0.07	C[8]	0.48	C	0.33	C	0.4	C

Figures:

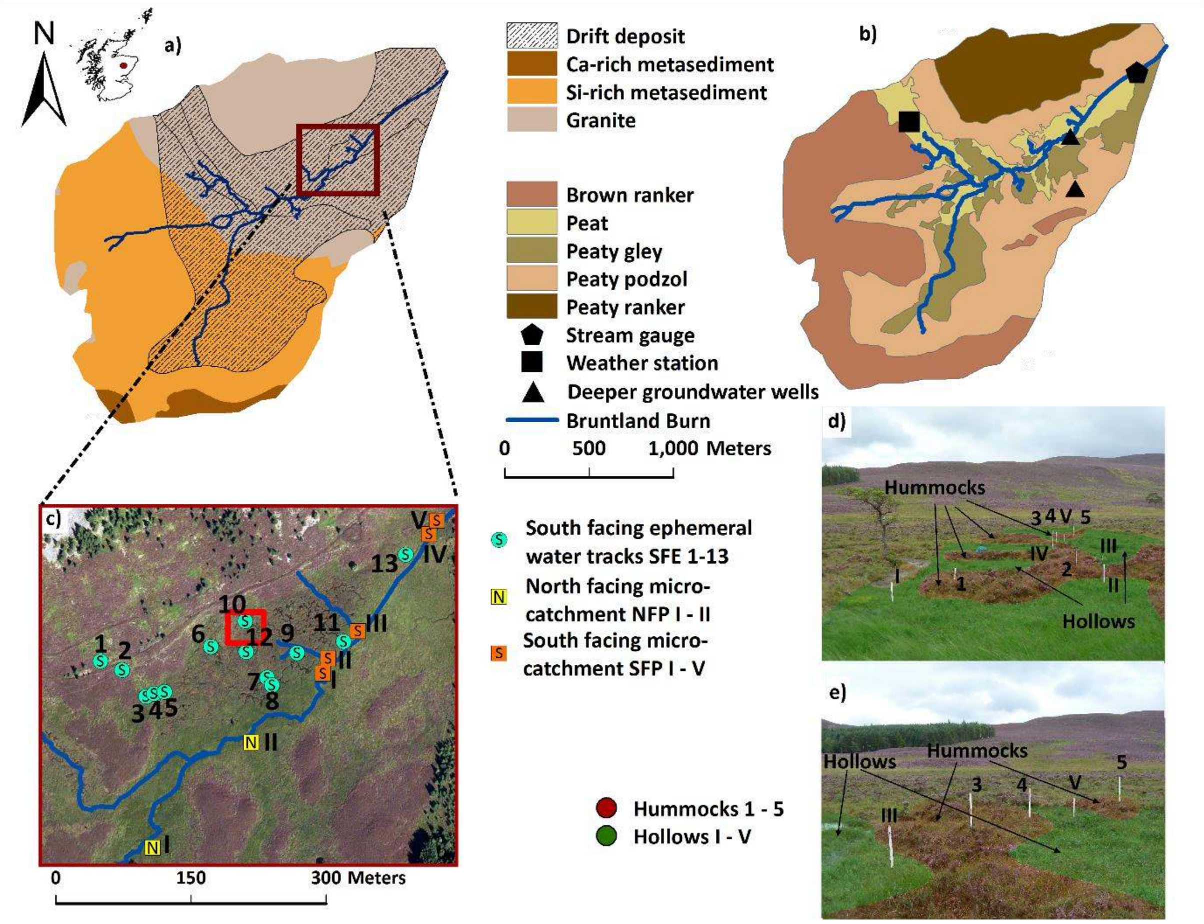

Figure 1: a) The underlying bedrock with the extent of the drift deposits and b) the soil map of the Bruntland Burn catchment; c) Sample locations (outlets) of the north facing perennial micro-catchment (NFP I-II, yellow squares), the south facing perennial micro-catchments (SFP I - V, orange squares) and south facing ephemeral water tracks (SFE 1 – 13, green circles) leading to the stream; the red square indicates the location of the micro-topography well cluster; the purple structures are large heather cover hummocky moraines; d) & f) photos of the micro-topography well cluster with wells insight the micro-topography features hummocks (reddish) and hollows (green).

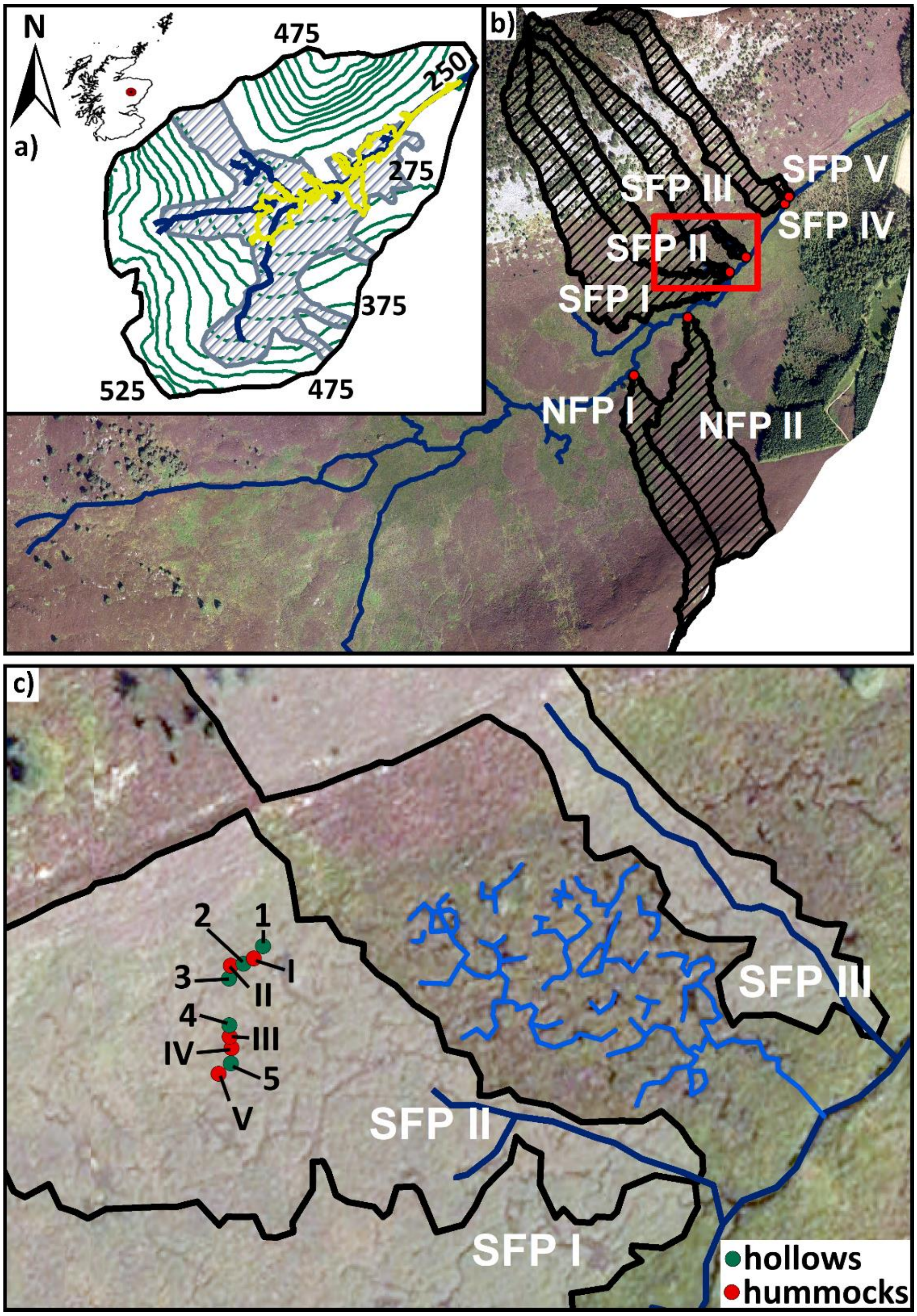

Figure 2: a) Topography of the Bruntlund Burn in 25 m increments and the minimal (yellow) and maximal (grey) extent of the saturated area; b) Catchment areas of the mirco-catchments; c) detailled field observation of the area between the SFP II and SFP III micro-catchments, concluding that the catchment delinenation from ArcGIS correct; Green (Hollow 1 - 5) and red (Hummock I - V) circles represent the locations of the the micro-topography wells inside SFP II's catchment.

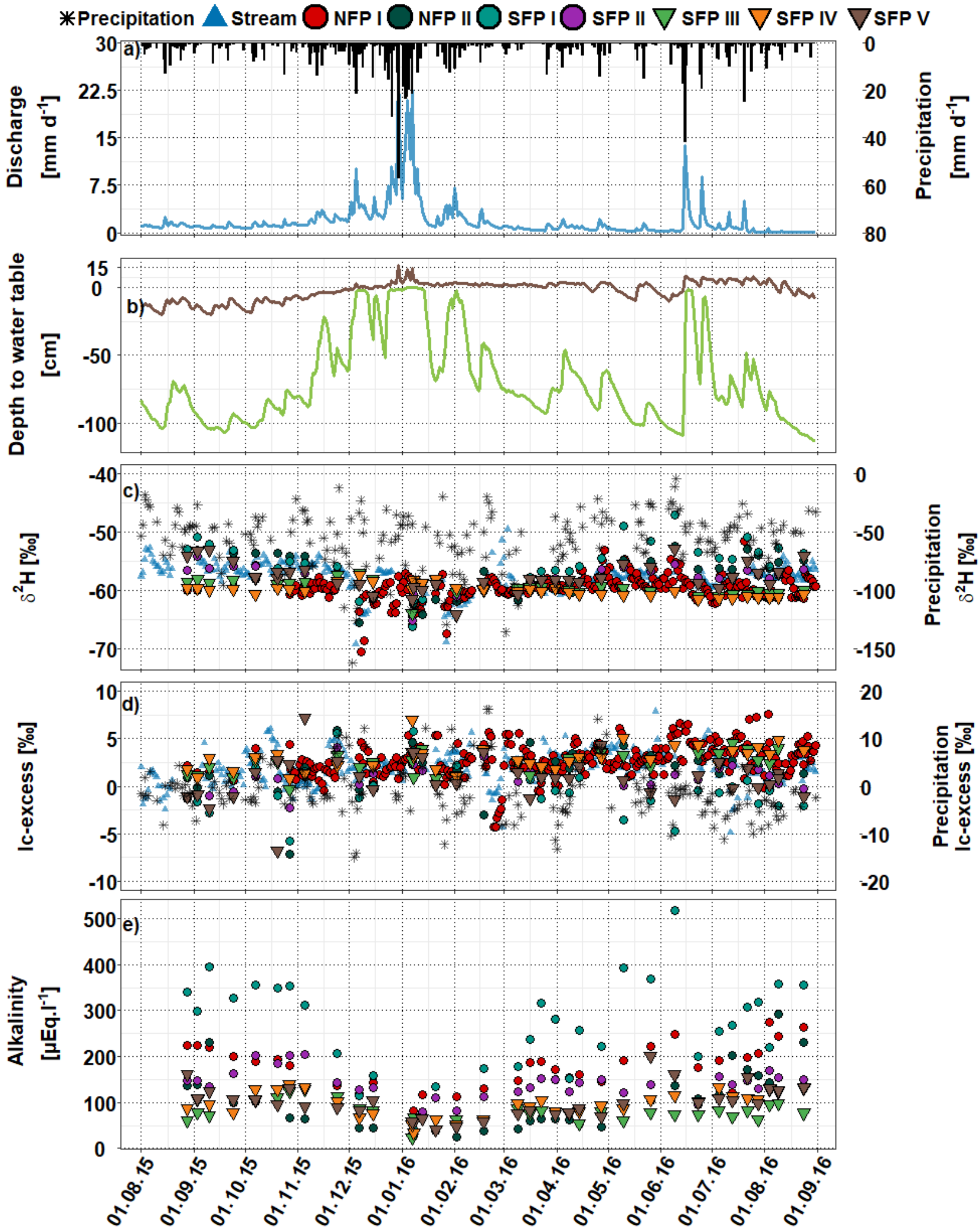

Figure 3: a) Daily precipitation and discharge at the catchment outlet; b) Groundwater time series from the riparian zone (brown) and the upper hillslope (green); c) δ^2H values from the sampled north and south-facing micro-catchments (NFP I, II, SFP I- V) together with the isotopic composition of the stream water and the precipitation (2nd y-axis); d) lc-excess for all perennial channel samples from the micro-catchments, the stream and the precipitation (2nd y-axis); e) alkalinity.

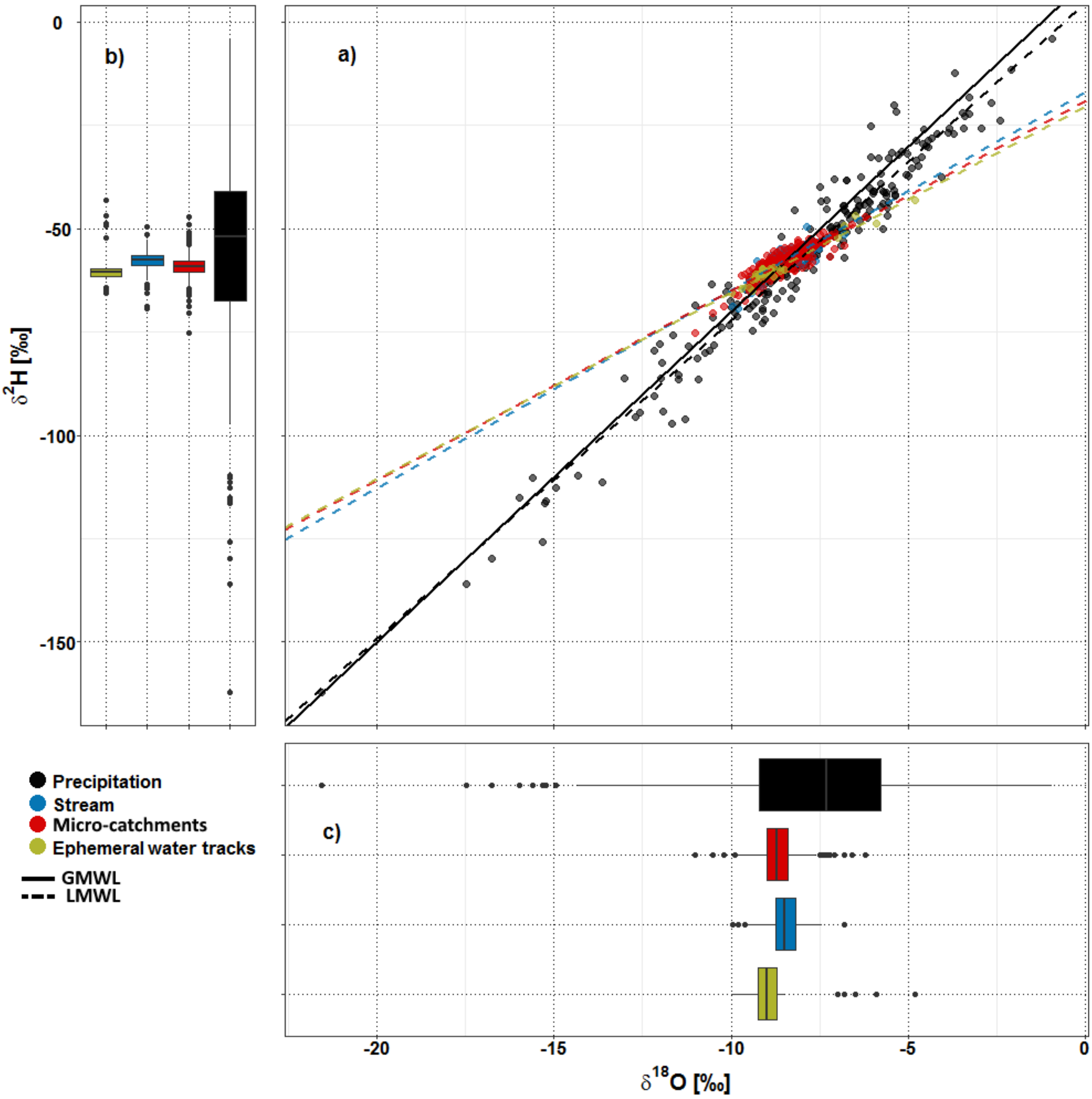

Figure 4: Isotopic composition of the collected precipitation samples (black) with the global (GMWL, black solid line) and the local meteoric water line (LMWL, black dashed line); and the stream water (SW) samples (blue), the samples from the perennial micro-catchment channels grouped together (red) and ephemeral water track (EWT) samples grouped together (green) with their respective regression lines (below caption); All circles are half-transparent to emphasis overlapping values; a) Samples of difference sources during the study period from the 1st August 2015 – 31st August 2016; b) boxplot of δ^2H; c) the boxplots of δ^{18}O values; Equations of the regression lines can be found in the supplementary Table S2.

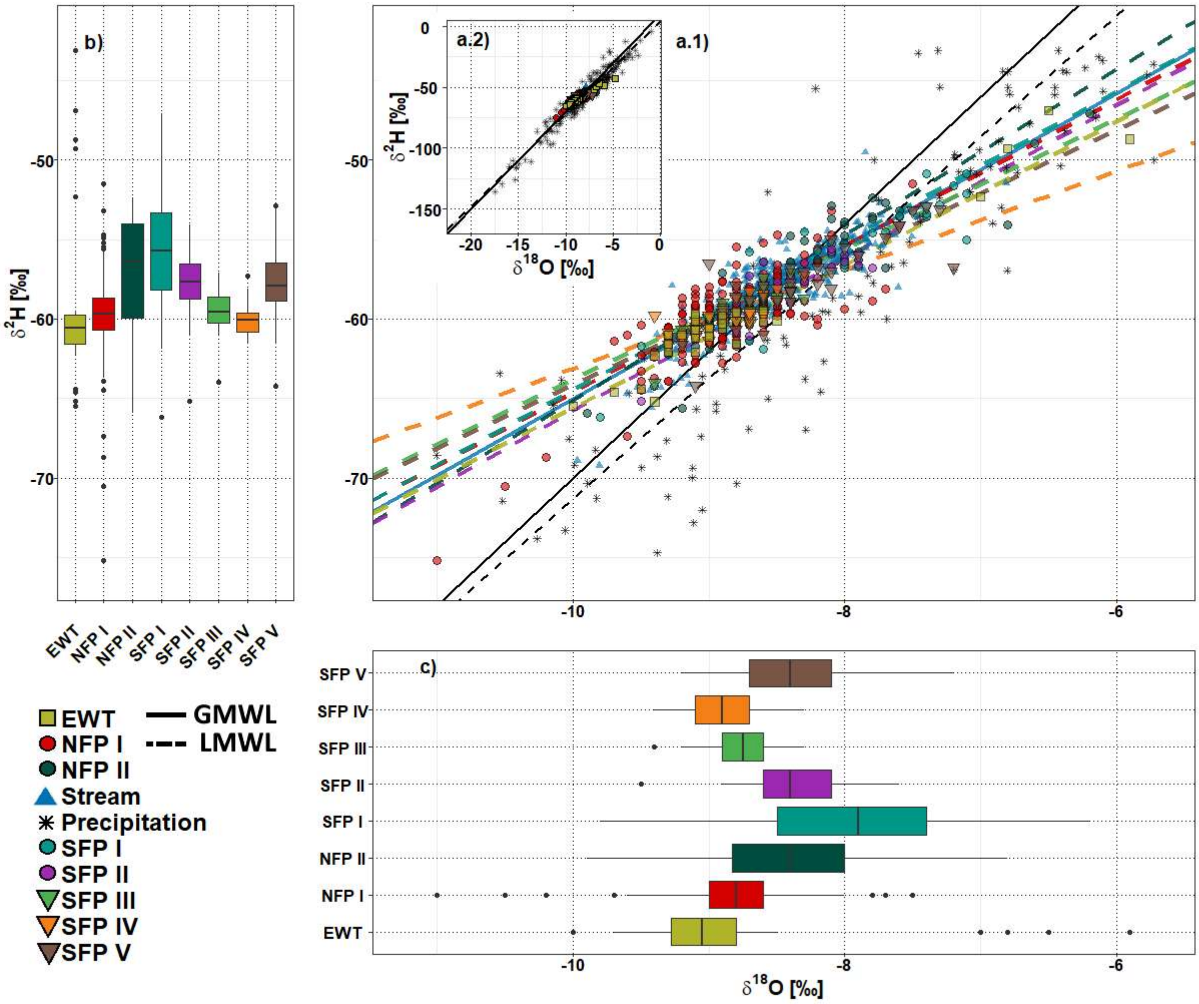

Figure 5: Water samples from the catchment during the study period from the 1st August 2015 – 31st August 2016 shown in a dual-isotope plot including the global (GMWL, black solid line) and local meteoric water line (LWML, black dashed line) and supplemented by the respective boxplots for δ^2H (b, left) and δ^{18}O (c, bottom); a.1) enlarged dual-Isotope plot with the respective regression lines for precipitation (black), stream water (SW, blue), NFP I (red), NFP II (dark green), SFP I (turquoise), SFP II (purple), SFP III (green) SFP IV (orange), SFP V (brown); all circles are half-transparent to emphasis overlapping values; a.2) shows the full isotopic range in the precipitation. Equations of the regression lines can be found in the supplementary Table S2.

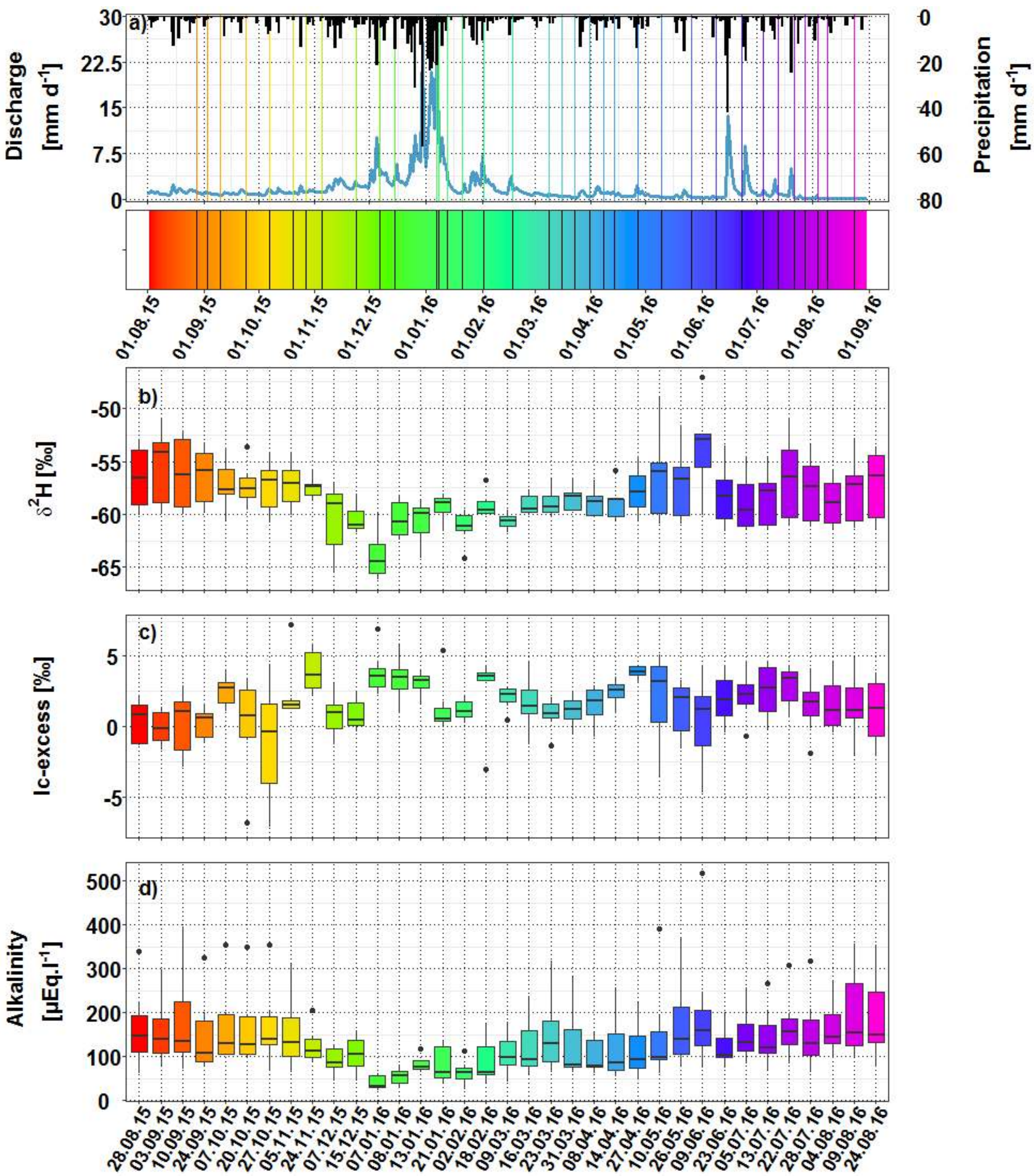

Figure 6: a) Daily precipitation and discharge for the study period with vertical lines indicating the 35 sampling dates for the micro-catchments, the line colours of each sampling date in a) corresponds to the colours of the boxplots for b) δ²H, c) lc-excess and d) alkalinity indicating the individual sampling dates of the micro-catchments.

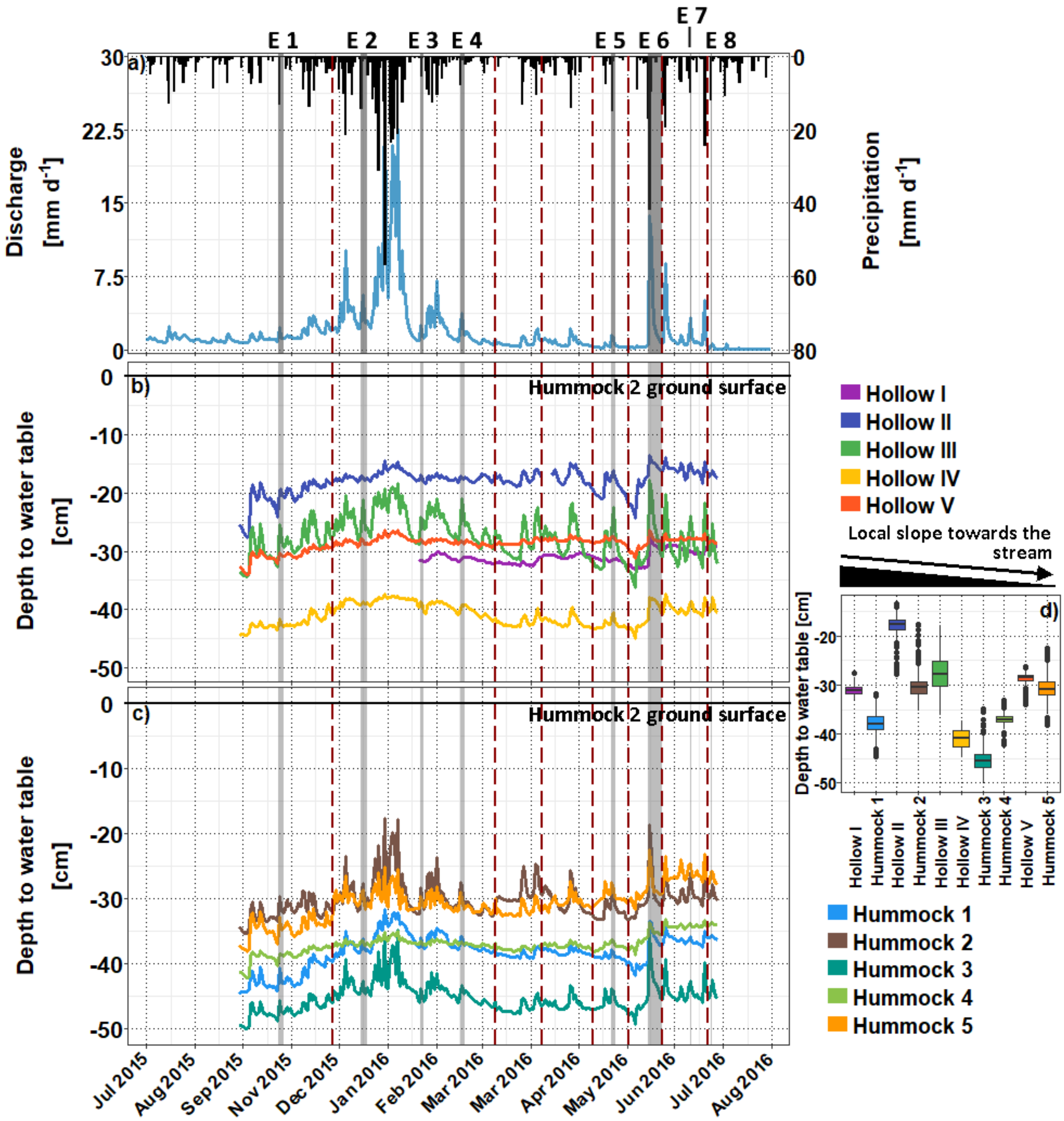

Figure 7: a) Daily precipitation and discharge; levelled groundwater levels b) insight the hollows; and c) insight the hummocks. 0 cm represent the ground surface of Hummock 2 which had the highest elevation of all micro-topography wells and serves as reference height for the wells. The inset d) shows boxplots of the water table inside the wells in the different micro-topography features sorted from highest to lowest location in respect to the local slope towards the stream. The vertical red dashed lines indicate the sampling dates. The grey vertical rectangles indicate the dates of the hysteresis events (E 1 to E 8).

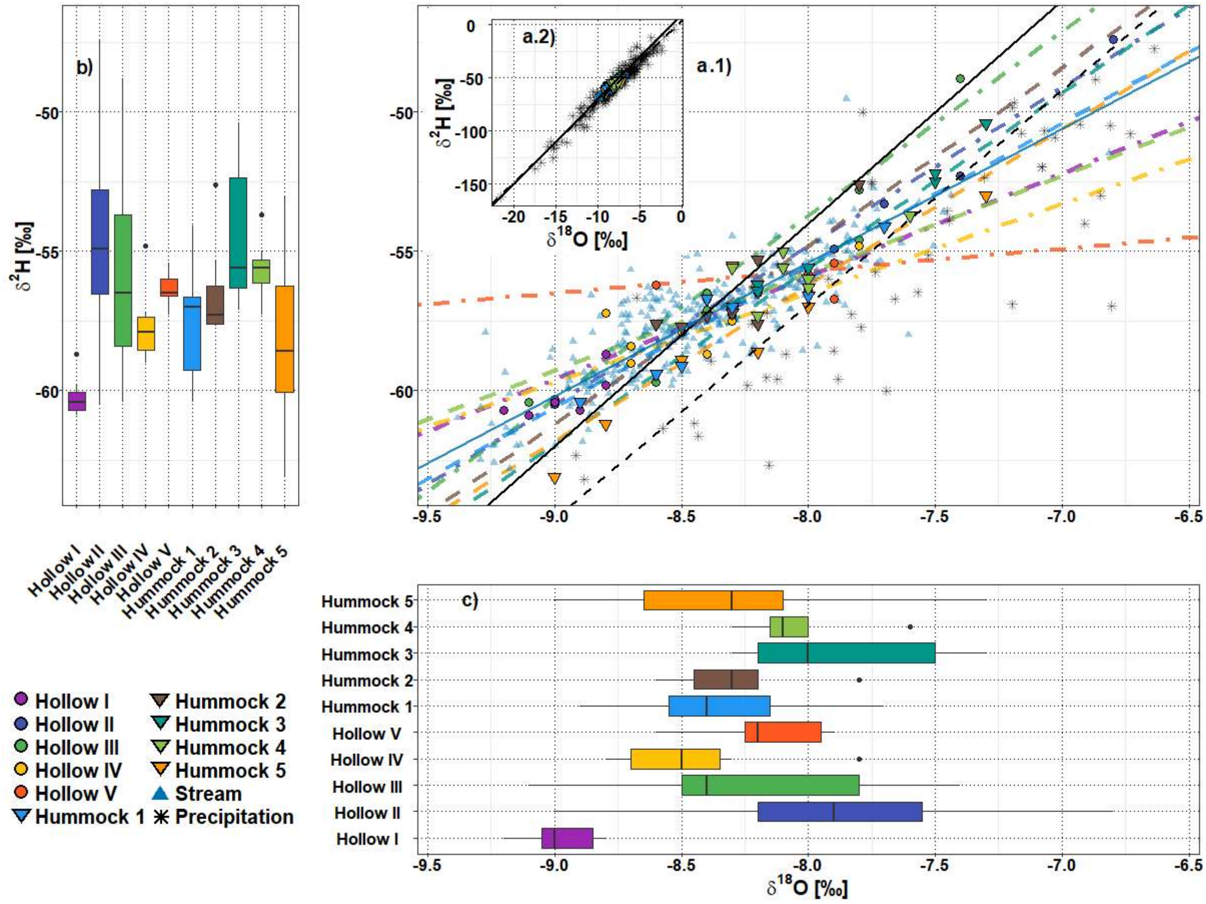

Figure 8: Water samples from the micro-topography wells from 1st August 2015 – 31st August 2016 including the global (GMWL, black solid line) and local meteoric water line (LWML, black dashed line) and boxplots for δ^2H (b) and $\delta^{18}O$ (c); a.1) enlarged plot with the respective regression lines for precipitation (black), stream water (SW, blue), Hollow I (purple), Hollow II (dark blue), Hollow III (green), Hollow IV (yellow), Hollow V (dark orange), Hummock 1 (light blue), Hummock 2 (brown), Hummock 3 (dark green), Hummock 4 (light green), Hummock 5 (orange); a.2) shows the full isotopic range in precipitation; all circles are half-transparent to emphasise overlapping values. Equations of the regression lines can be found in the supplementary Table S2.

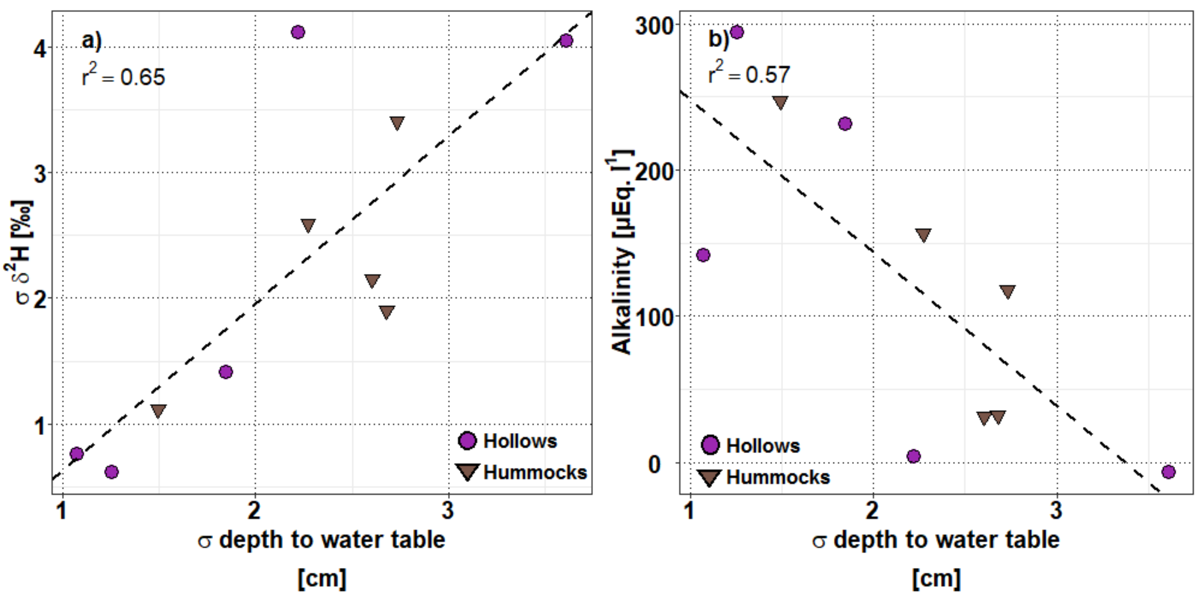

Figure 9: Relationships for the micro-topography wells between a) the standard deviations of the depth to water table values vs the standard deviations of their δ^2H values with regression line ($y = 1.34x - 0.7$, $R^2 = 0.65$, $p < 0.005$) and, b) the standard deviations of the depth to water table values vs alkalinity with regression line ($y = -104.93x + 353.6$, $R^2 = 0.57$, $p < 0.05$).

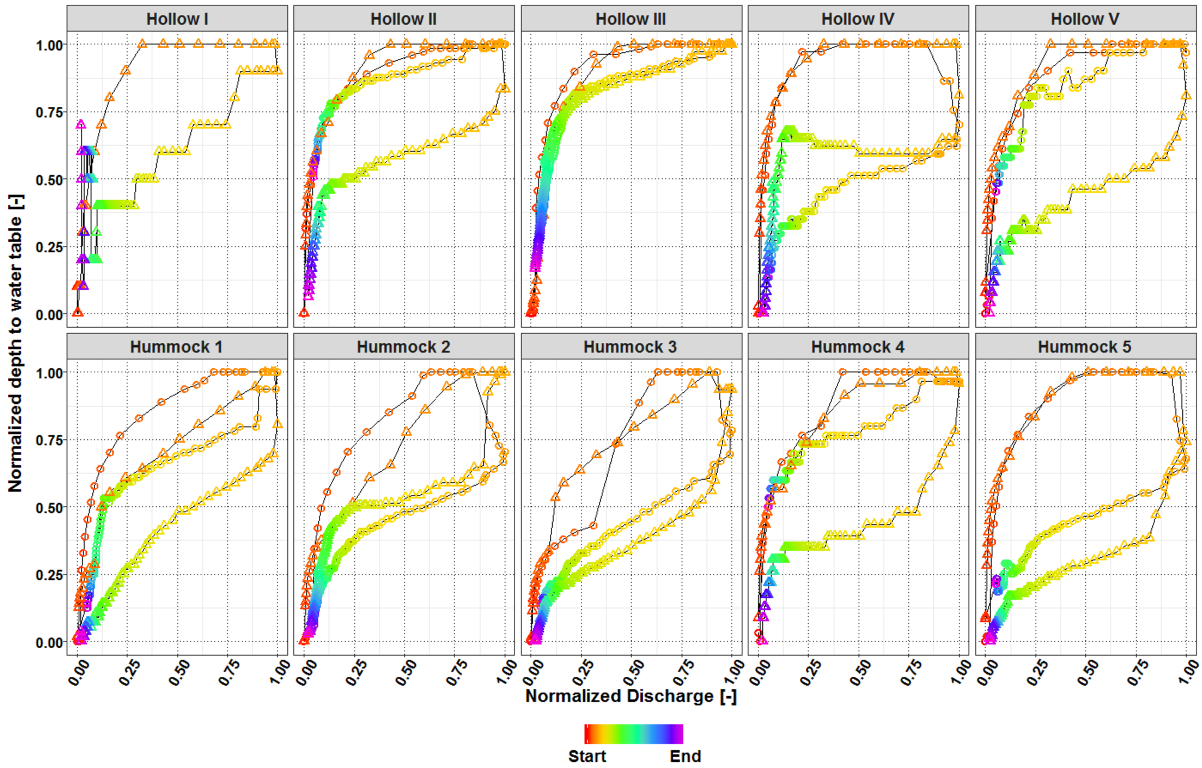

Figure 10: Hysteresis plots of normalized stream discharge vs depth to water tables during event 1 (circles) between October 24th – October 27th 2015 and event 5 (triangles) between May 22nd– May 25th2016; The logger in Hollow 1 was malfunctioning during event 1.

Reference

Acreman M, Holden J. 2013. How wetlands affect floods. *Wetlands* **33** (5): 773–786 DOI: 10.1007/s13157-013-0473-2

Ala-aho P, Soulsby C, Wang H, Tetzlaff D. 2017. Integrated surface-subsurface model to investigate the role of groundwater in headwater catchment runoff generation: A minimalist approach to parameterisation. *Journal of Hydrology* **547**: 664–677 DOI: 10.1016/j.jhydrol.2017.02.023

Banner A, MacKenzie W. 1998. Riparian Areas: Providing Landscape Habitat Diversity Part 5 of 7. Smithers.

Barthold FK, Tyralla C, Schneider K, Vaché KB, Frede H-G, Breuer L. 2011. How many tracers do we need for end member mixing analysis (EMMA)? A sensitivity analysis. *Water Resources Research* **47** (8) DOI: 10.1029/2011WR010604

Belyea LR, Clymo RS. 2001. Feedback control of the rate of peat formation. *Proceedings of the Royal Society B: Biological Sciences* **268** (1473): 1315–1321 DOI: 10.1098/rspb.2001.1665

Birkel C, Soulsby C, Tetzlaff D. 2011a. Modelling catchment-scale water storage dynamics: reconciling dynamic storage with tracer-inferred passive storage. *Hydrological Processes* **25** (25): 3924–3936 DOI: 10.1002/hyp.8201

Birkel C, Tetzlaff D, Dunn SM, Soulsby C. 2011b. Using time domain and geographic source tracers to conceptualize streamflow generation processes in lumped rainfall-runoff models. *Water Resources Research* **47** (2) DOI: 10.1029/2010WR009547

Blumstock M, Tetzlaff D, Dick JJ, Nuetzmann G, Soulsby C. 2016. Spatial organization of groundwater dynamics and streamflow response from different hydropedological units in a montane catchment. *Hydrological Processes* **30** (21): 3735–3753 DOI: 10.1002/hyp.10848

Blumstock M, Tetzlaff D, Malcolm IA, Nuetzmann G, Soulsby C. 2015. Baseflow dynamics: Multi-tracer surveys to assess variable groundwater contributions to montane streams under low flows. *Journal of Hydrology* **527**: 1021–1033 DOI: 10.1016/j.jhydrol.2015.05.019

Bragg OM. 2002. Hydrology of peat-forming wetlands in Scotland. *Science of the Total Environment* **294** (1–3): 111–129 DOI: 10.1016/S0048-9697(02)00059-1

Bullock A, Acreman M. 2003. The role of wetlands in the hydrological cycle. *Hydrology and Earth System Sciences* **7** (3): 358–389 DOI: 10.5194/hess-7-358-2003

Chimner RA, Hart JB. 1996. Hydrology and microtopography effects on northern white-cedar regeneration in Michigan's Upper Peninsula. *Canadian Journal of Forest Research* **26** (3): 389–393 DOI: 10.1139/x26-043

Coplen TB. 2011. Guidelines and recommended terms for expression of stable-isotope-ratio and gas-ratio measurement results. *Rapid Communications in Mass Spectrometry* **25** (17): 2538–2560 DOI: 10.1002/rcm.5129

Correa A, Windhorst D, Tetzlaff D, Crespo P, Célleri R, Feyen J, Breuer L. 2017. Temporal dynamics in dominant runoff sources and flow paths in the Andean Páramo. *Water Resources Research* **53** (7): 5998–6017 DOI: 10.1002/2016WR020187

Craig H, Gordon LI, Horibe Y. 1963. Isotopic exchange effects in the evaporation of water: 1. Low-temperature experimental results. *Journal of Geophysical Research* **68** (17): 5079–5087 DOI: 10.1029/JZ068i017p05079

Dansgaard W. 1964. Stable isotopes in precipitation. *Tellus* **16** (4): 436–468 DOI: 10.3402/tellusa.v16i4.8993

Devito KJ, Hokanson KJ, Moore PA, Kettridge N, Anderson AE, Chasmer L, Hopkinson C, Lukenbach MC, Mendoza CA, Morissette J, Peters DL, Petrone RM, Silins U, Smerdon B, Waddington JM. 2017. Landscape controls on long-term runoff in subhumid heterogeneous Boreal Plains catchments. *Hydrological Processes* **31** (15): 2737–2751 DOI: 10.1002/hyp.11213

Didszun J, Uhlenbrook S. 2008. Scaling of dominant runoff generation processes: Nested catchments approach using multiple tracers. *Water Resources Research* **44** (2): 1–15 DOI: 10.1029/2006WR005242

Eppinga MB, Rietkerk M, Borren W, Lapshina ED, Bleuten W, Wassen MJ. 2008. Regular surface patterning of peatlands: Confronting theory with field data. *Ecosystems* **11** (4): 520–536 DOI: 10.1007/s10021-008-9138-z

Esteves M, Faucher X, Galle S, Vauclin M. 2000. Overland flow and infiltration modelling for small plots during unsteady rain: Numerical results versus observed values. *Journal of Hydrology* **228** (3–4): 265–282 DOI: 10.1016/S0022-1694(00)00155-4

Fiedler FR, Ramirez JA. 2000. A numerical method for simulating discontinuous shalloe flow over and infiltrating surface. *International Journal for Numerical Methods in Fluids* **32** (6): 219–240 Available at: http://dx.doi.org/10.1002/(SICI)1097-0363(20000130)32:2%3C219::AID-FLD936%3E3.0.CO;2-J

Fischer BMC, Rinderer M, Schneider P, Ewen T, Seibert J. 2015. Contributing sources to baseflow in pre-alpine headwaters using spatial snapshot sampling. *Hydrological Processes* **29** (26): 5321–5336 DOI: 10.1002/hyp.10529

Frei S, Fleckenstein JH. 2014. Representing effects of micro-topography on runoff generation and sub-surface flow patterns by using superficial rill/depression storage height variations. *Environmental Modelling and Software* **52**: 5–18 DOI: 10.1016/j.envsoft.2013.10.007

Frei S, Lischeid G, Fleckenstein JH. 2010. Effects of micro-topography on surface-subsurface exchange and runoff generation in a virtual riparian wetland - A modeling study. *Advances in Water Resources* **33** (11): 1388–1401 DOI: 10.1016/j.advwatres.2010.07.006

Von Freyberg J, Radny D, Gall HE, Schirmer M. 2014. Implications of hydrologic connectivity between hillslopes and riparian zones on streamflow composition. *Journal of Contaminant Hydrology* **169**: 62–74 DOI: 10.1016/j.jconhyd.2014.07.005

Geris J, Tetzlaff D, McDonnell JJ, Soulsby C. 2015. The relative role of soil type and tree cover on water storage and transmission in northern headwater catchments. *Hydrological Processes* **29** (7): 1844–1860 DOI: 10.1002/hyp.10289

Gilman K. 1994. *Hydrology and Wetland Conservation*. Wiley. Available at: https://books.google.co.uk/books?id=CVbuAAAAMAAJ

González E, Felipe-Lucia MR, Bourgeois B, Boz B, Nilsson C, Palmer G, Sher AA. 2016. Integrative conservation of riparian zones. *Biological Conservation* DOI: 10.1016/j.biocon.2016.10.035

van Huijgevoort MHJ, Tetzlaff D, Sutanudjaja EH, Soulsby C. 2016. Using high resolution tracer data to constrain water storage, flux and age estimates in a spatially distributed rainfall-runoff model. *Hydrological Processes* **30** (25): 4761–4778 DOI: 10.1002/hyp.10902

Jencso KG, McGlynn BL, Gooseff MN, Bencala KE, Wondzell SM. 2010. Hillslope hydrologic connectivity controls riparian groundwater turnover: Implications of catchment structure for riparian buffering and stream water sources. *Water Resources Research* **46** (10): 1–18 DOI: 10.1029/2009WR008818

Jenson SK, Domingue JO. 1988. Extracting topographic structure from digital elevation data for geographic information system analysis. *Photogrammetric Engineering and Remote Sensing* **54** (11): 1593–1600 DOI: 0099-1112/88/5411-1593$02.25/0

Kendall C, McDonnell JJ. 1998. *Isotope Tracers in Catchment Hydrology*. Elsevier sciene: Amsterdam.

Kenkel NC. 1988. Spectral analysis of hummock-hollow pattern in a weakly minerotrophic mire. *Vegetatio* **78** (1–2): 45–52 DOI: 10.1007/BF00045638

Klaus J, McDonnell JJ, Jackson CR, Du E, Griffiths NA. 2015. Where does streamwater come from in low-relief forested watersheds? A dual-isotope approach. *Hydrology and Earth System Sciences* **19** (1): 125–135 DOI: 10.5194/hess-19-125-2015

Kværner J, Kløve B. 2006. Tracing sources of summer streamflow in boreal headwaters using isotopic signatures and water geochemical components. *Journal of Hydrology* **331** (1–2): 186–204 DOI: 10.1016/j.jhydrol.2006.05.008

Landwehr JM, Coplen TB. 2006. Line-conditioned excess: a new method for characterizing stable hydrogen and oxygen isotope ratios in hydrologic systems. In *Isotopes in Environmental Studies - Aquatic Forum 2004*IAEA; 132–135.

Leibundgut C, Maloszewski P, Külls C. 2009. *Tracers in Hydrology*. John Wiley & Sons.

Lessels JS, Tetzlaff D, Birkel C, Dick JJ, Soulsby C. 2016. Water sources and mixing in riparian wetlands revealed by tracers and geospatial analysis. *Water Resources Research* **52** (1): 456–470 DOI: 10.1002/2015WR017519

Lloyd CEM, Freer JE, Johnes PJ, Collins AL. 2016. Technical Note: Testing an improved index for analysing storm discharge–concentration hysteresis. *Hydrology and Earth System Sciences* **20** (2): 625–632 DOI: 10.5194/hess-20-625-2016

Malhotra A, Roulet NT, Wilson P, Giroux-Bougard X, Harris LI. 2016. Ecohydrological feedbacks in peatlands: an empirical test of the relationship among vegetation, microtopography and water table. *Ecohydrology* **9** (7): 1346–1357 DOI: 10.1002/eco.1731

McDonnell JJ, McGlynn BL, Kendall K, Shanley JB, Kendall C. 1998. The role of near-stream riparian zones in the hydrology of steep upland catchments. *IAHS-AISH Publication* **248**: 173–180 Available at: http://pubs.er.usgs.gov/publication/70020116

McGlynn BL, McDonnell JJ. 2003. Quantifying the relative contributions of riparian and hillslope zones to catchment runoff. *Water Resour. Res.* **39** (11): 1310 DOI: 10.1029/2003wr002091

McGlynn BL, Mcdonnell JJ, Seibert J, Kendall C. 2004. Scale effects on headwater catchment runoff timing, flow sources, and groundwater-streamflow relations. *Water Resources Research* **40** (April): 1–14 DOI: 10.1029/2003WR002494

van Meerveld HJ, Seibert J, Peters NE. 2015. Hillslope-riparian-stream connectivity and flow directions at the Panola Mountain Research Watershed. *Hydrological Processes* **29** (16): 3556–3574 DOI: 10.1002/hyp.10508

Naiman RJ, Decamps H. 1997. The ecology of interfases: Riparian Zones. *Annual Review of Ecology, Evolution, and Systematics* **28** (102): 621–658 DOI: 10.1146/annurev.ecolsys.28.1.621

Neal C. 2001. Alkalinity measurements within natural waters: towards a standardised approach. *Science of The Total Environment* **265** (1–3): 99–113 DOI: 10.1016/S0048-9697(00)00652-5

Neal C, Hill T, Hill S, Reynolds B. 1997. Acid neutralization capacity measurements in surface and ground waters in the Upper River Severn, Plynlimon: from hydrograph splitting to water flow pathways. *Hydrology and Earth System Sciences* **1** (3): 687–696 DOI: 10.5194/hess-1-687-1997

Partington D, Brunner P, Frei S, Simmons CT, Werner AD, Therrien R, Maier HR, Dandy GC, Fleckenstein JH. 2013. Interpreting streamflow generation mechanisms from integrated surface-subsurface flow models of a riparian wetland and catchment. *Water Resources Research* **49** (9): 5501–5519 DOI: 10.1002/wrcr.20405

Penna D, van Meerveld HJ, Oliviero O, Zuecco G, Assendelft R, Dalla Fontana G, Borga M. 2015. Seasonal changes in runoff generation in a small forested mountain catchment. *Hydrological Processes* **29** (8): 2027–2042 DOI: 10.1002/hyp.10347

Penna D, van Meerveld HJ, Zuecco G, Dalla Fontana G, Borga M. 2016. Hydrological response of an Alpine catchment to rainfall and snowmelt events. *Journal of Hydrology* **537**: 382–397 DOI: 10.1016/j.jhydrol.2016.03.040

Peralta-Tapia A, Sponseller RA, Ågren A, Tetzlaff D, Soulsby C, Laudon H. 2015. Scale-dependent groundwater contributions influence patterns of winter baseflow stream chemistry in boreal catchments. *Journal of Geophysical Research: Biogeosciences* **120** (5): 847–858 DOI: 10.1002/2014JG002878

Van der Ploeg MJ, Appels WM, Cirkel DG, Oosterwoud MR, Witte J-PM, van der Zee SEATM. 2012. Microtopography as a Driving Mechanism for Ecohydrological Processes in Shallow Groundwater Systems. *Vadose Zone Journal* **11** (3): 0 DOI: 10.2136/vzj2011.0098

Qu Y, Duffy CJ. 2007. A semidiscrete finite volume formulation for multiprocess watershed simulation. *Water Resources Research* **43** (8): 1–18 DOI: 10.1029/2006WR005752

R Core Team. 2017. R: A language and environment for statistical computing. *R Found. for Stat. Comput., Vienna* Available at: https://www.r-project.org

Rietkerk M, Dekker SC, Wassen MJ, Verkroost a WM, Bierkens MFP. 2004. A putative mechanism for bog patterning. *The American naturalist* **163** (5): 699–708 DOI: 10.1086/383065

Šanda M, Vitvar T, Kulasová A, Jankovec J, Císlerová M. 2014. Run-off formation in a humid, temperate headwater catchment using a combined hydrological, hydrochemical and isotopic approach (Jizera Mountains, Czech Republic). *Hydrological Processes* **28** (8): 3217–3229 DOI: 10.1002/hyp.9847

Scheliga B, Tetzlaff D, Nuetzmann G, Soulsby C. 2017. Groundwater isoscapes in a montane headwater catchment show dominance of well-mixed storage. *Hydrological Processes* **31** (March): 1–16 DOI: 10.1002/hyp.11271

Shi X, Thornton PE, Ricciuto DM, Hanson PJ, Mao J, Sebestyen SD, Griffiths NA, Bisht G. 2015. Representing northern peatland microtopography and hydrology within the Community Land Model. *Biogeosciences* **12** (21): 6463–6477 DOI: 10.5194/bg-12-6463-2015

Soulsby C, Birkel C, Geris J, Dick JJ, Tunaley C, Tetzlaff D. 2015. Stream water age distributions controlled by storage dynamics and nonlinear hydrologic connectivity: Modeling with high-resolution isotope data. *Water Resources Research* **51** (9): 7759–7776 DOI: 10.1002/2015WR017888

Soulsby C, Bradford J, Dick JJ, McNamara JP, Geris J, Lessels JS, Blumstock M, Tetzlaff D. 2016. Using geophysical surveys to test tracer-based storage estimates in headwater catchments. *Hydrological Processes* (April) DOI: 10.1002/hyp.10889

Soulsby C, Dick J, Scheliga B, Tetzlaff D. 2017. Taming the flood-How far can we go with trees? *Hydrological Processes* **31** (17): 3122–3126 DOI: 10.1002/hyp.11226

Soulsby C, Tetzlaff D, van den Bedem N, Malcolm IA, Bacon PJ, Youngson AF. 2007. Inferring groundwater influences on surface water in montane catchments from hydrochemical surveys of springs and streamwaters. *Journal of Hydrology* **333** (2–4): 199–213 DOI: 10.1016/j.jhydrol.2006.08.016

Sprenger M, Tetzlaff D, Tunaley C, Dick JJ, Soulsby C. 2017. Evaporation fractionation in a peatland drainage network affects stream water isotope composition. *Water Resources Research* **53** (1): 851–866 DOI: 10.1002/2016WR019258

Sun H, Kasahara T, Otsuki K, Saito T, Onda Y. 2016. Spatio-temporal streamflow generation in a small, steep headwater catchment in western Japan. *Hydrological Sciences Journal* **62** (5): 1–12 DOI: 10.1080/02626667.2016.1266635

Tetzlaff D, Soulsby C. 2008. Sources of baseflow in larger catchments – Using tracers to develop a holistic understanding of runoff generation. *Journal of Hydrology* **359** (3–4): 287–302 DOI: 10.1016/j.jhydrol.2008.07.008

Tetzlaff D, Birkel C, Dick JJ, Geris J, Soulsby C. 2014. Storage dynamics in hydropedological units control hillslope connectivity, runoff generation, and the evolution of catchment transit time distributions. *Water Resources Research* **50** (2): 969–985 DOI: 10.1002/2013WR014147

Tetzlaff D, Capell R, Soulsby C. 2012. Land use and hydroclimatic influences on Faecal Indicator Organisms in two large Scottish catchments: Towards land use-based models as screening tools. *Science of The Total Environment* **434**: 110–122 DOI: 10.1016/j.scitotenv.2011.11.090

Tetzlaff D, Soulsby C, Bacon PJ, Youngson AF, Gibbins C, Malcolm IA. 2007a. Connectivity between landscapes and riverscapes—a unifying theme in integrating hydrology and ecology in catchment science? *Hydrological Processes* **21** (10): 1385–1389 DOI: 10.1002/hyp.6701

Tetzlaff D, Soulsby C, Waldron S, Malcolm IA, Bacon PJ, Dunn SM, Lilly A, Youngson AF. 2007b. Conceptualization of runoff processes using a geographical information system and tracers in a nested mesoscale catchment. *Hydrological Processes* **21** (10): 1289–1307 DOI: 10.1002/hyp.6309

Tetzlaff D, Uhlenbrook S, Eppert S, Soulsby C. 2008. Does the incorporation of process conceptualization and tracer data improve the structure and performance of a simple rainfall-runoff model in a Scottish mesoscale catchment? *Hydrological Processes* **22** (14): 2461–2474 DOI: 10.1002/hyp.6841

Tunaley C, Tetzlaff D, Soulsby C. 2017. Scaling effects of riparian peatlands on stable isotopes in runoff and DOC mobilization. *Journal of Hydrology* **In review**: 220–235 DOI: 10.1016/j.jhydrol.2017.03.056

Vidon PGF. 2017. Not all riparian zones are wetlands: Understanding the limitation of the "wetland bias" problem. *Hydrological Processes* (February): 3–5 DOI: 10.1002/hyp.11153

Wang H, Tetzlaff D, Dick JJ, Soulsby C. 2017. Assessing the environmental controls on Scots pine transpiration and the implications for water partitioning in a boreal headwater catchment. *Agricultural and Forest Meteorology* **240**–**241** (November 2016): 58–66 DOI: 10.1016/j.agrformet.2017.04.002

Appendix – Supplementary Tables

Table S1: Identified moss species with their usual place of occurrence and its general chemistry according to literature; and field observations near which well they were identified as well as the mean water level insight the respective well.

Species	Habitat	Chemistry	Places	Micro-topography feature	mean water level below ground surface [cm]	dominate feature
Sphagnum fimbriatum	damp places(bbsfieldguide)	moderately enriched with nutrients (bbsfieldguide)	fens, juncus mires (bbsfieldguide)	Hummock 1	-29	Hummock
	hummock, lawn (Vitt, 2014)	moderate-rich fens, pH 6-8 (Vitt 2014)		Hummock 2	-30.6	
				Hummock 3	-32.2	
				Hummock 4	-15	
Sphagnum capillifolium subs. capillifolium	well-drained mineral soil, shallow peat in humid places, Heather dominated banks (bbsfieldguide)	poor in fens with low Ca, electric conductivity, Mg (Gignac & Vitt, 1990)	bogs, heathlands (bbsfieldguide)	Hummock 4	-15	Hummock
	hummock(Vitt, 2014)	poor and rich fens, pH 3-5 (Vitt, 2014)		Hummock 5	-29.4	
				Hollow III	-12.3	
Warnstorfia sarmentosa	near flushes, springs (bbsfieldguide)	base-rich, mineral rich fens (bbsfieldguide)		Hollow I	-0.1	Hollow
Sphagnum papillosum	beside flushes (bbsfieldguide)	poor fens, low Ca, electric conductivity, Mg (Gignac & Vitt, 1990)	raised/blanket bogs, mires (bbsfieldguide)	Hollow II	-5.8	Hollow
	lawn (Vitt, 2014)	poor fens, ph 4-6 (Vitt 2014)		Hollow IV	-2.5	
				Hollow V	4.7	
				Hummock 4	-15	

Table S2: Regressions equations for the linear relationships shown in the dual-isotope plots (Fig. 4, 5 and 9).

	Regression equations	r^2	Line colour and type	Figure
GMWL	$\delta^2H = 8 \times \delta^{18}O + 10$	-	black, solid line	4, 5, 9
LMWL	$\delta^2H = 7.6 \times \delta^{18}O + 4.7$	0.95	black, dashed line	4, 5, 9
SW	$\delta^2H = 4.8 \times \delta^{18}O - 17$	0.73	blue, solid line	4, 5, 9
Micro-catchments$_{grouped}$	$\delta^2H = 4.6 \times \delta^{18}O - 19.1$	0.72	red, dashed line	4
EWT	$\delta^2H = 4.5 \times \delta^{18}O - 20.6$	0.92	yellow, dashed line	4
NFP I	$\delta^2H = 4.6 \times \delta^{18}O - 18.6$	0.64	red, dashed line	5
NFP II	$\delta^2H = 5.2 \times \delta^{18}O - 13.1$	0.77	dark green, dashed line	5
SFP I	$\delta^2H = 4.7 \times \delta^{18}O - 17.5$	0.88	turquoise, dashed line	5
SFP II	$\delta^2H = 4.8 \times \delta^{18}O - 17.8$	0.8	purple, dashed line	5
SFP III	$\delta^2H = 4.1 \times \delta^{18}O – 22.8$	0.75	green, dashed line	5
SFP IV	$\delta^2H = 3.1 \times \delta^{18}O – 32.1$	0.63	orange, dashed line	5
SFP V	$\delta^2H = 4 \times \delta^{18}O – 24.1$	0.7	brown, dashed line	5
Hollow I	$\delta^2H = 3.7 \times \delta^{18}O – 26.3$	0.55	purple, dashed dotted line	9
Hollow II	$\delta^2H = 5.7 \times \delta^{18}O – 9.2$	0.95	dark blue, dashed dotted line	9
Hollow III	$\delta^2H = 6.6 \times \delta^{18}O – 0.9$	0.9	green, dashed dotted line	9
Hollow IV	$\delta^2H = 3.2 \times \delta^{18}O – 30.9$	0.6	yellow, dashed dotted line	9
Hollow V	$\delta^2H = 0.8 \times \delta^{18}O – 49.3$	0.1	dark orange, dashed dotted line	9
Hummock 1	$\delta^2H = 5.1 \times \delta^{18}O – 14.7$	0.9	light blue, dashed dotted line	9
Hummock 2	$\delta^2H = 6.4 \times \delta^{18}O – 3.6$	0.77	brown, dashed dotted line	9
Hummock 3	$\delta^2H = 6.3 \times \delta^{18}O – 5.2$	0.99	dark green, dashed dotted line	9
Hummock 4	$\delta^2H = 3.5 \times \delta^{18}O – 27.8$	0.74	light green, dashed dotted line	9
Hummock 5	$\delta^2H = 5.6 \times \delta^{18}O – 11.4$	0.86	orange, dashed dotted line	9

Appendix – Supplementary Figure

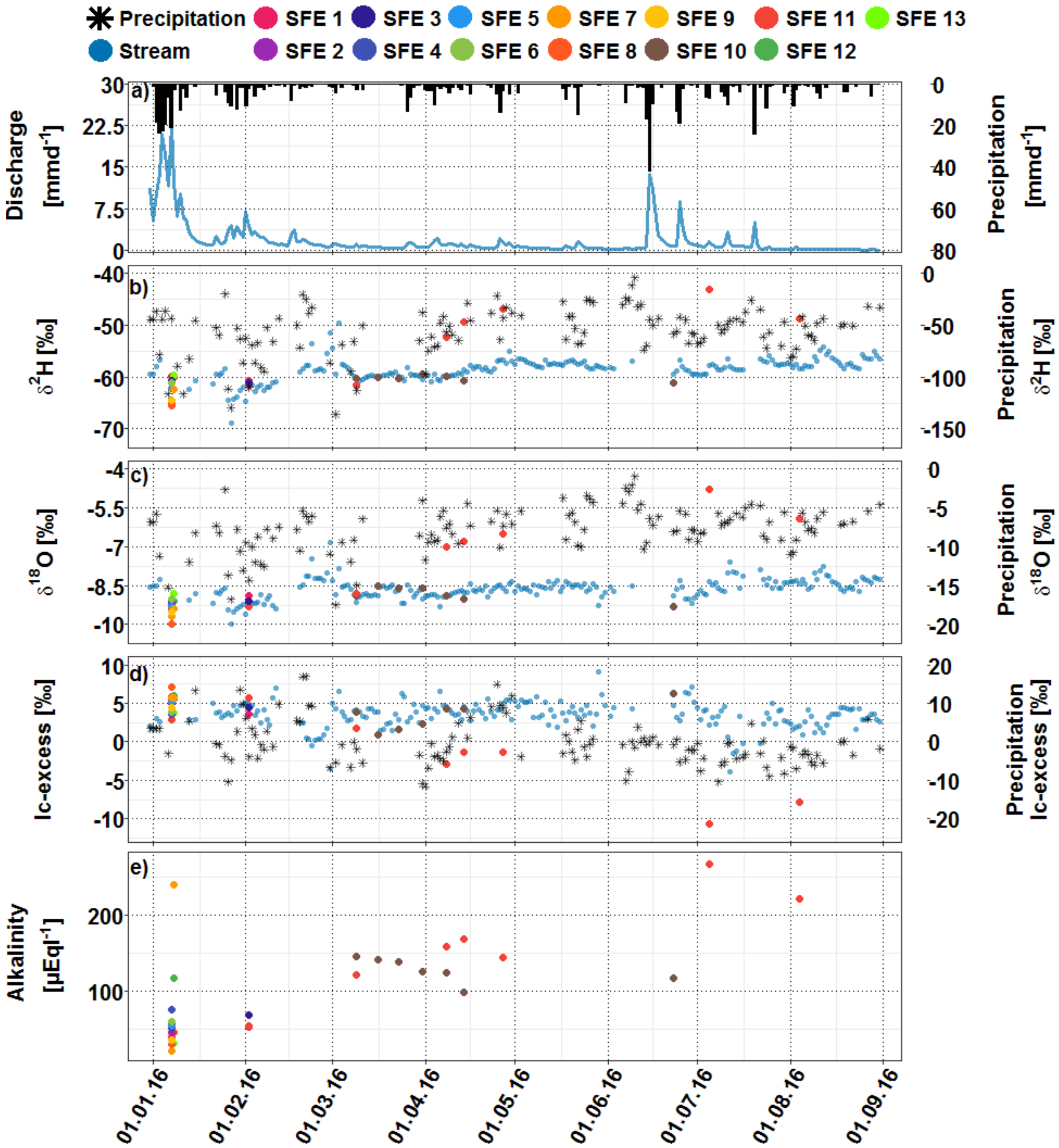

Figure S1: a) Daily precipitation and discharge, b) δ^2H, c) lc-excess and d) alkalinity of ephemeral water tracks in the catchment. Most ephemeral water tracks were only active as result of a succession of larger storm events during mid-December 2015 and early January 2016.